Article

Cell Reports

OXR1A, a Coactivator of PRMT5 Regulating Histone Arginine Methylation

Graphical Abstract

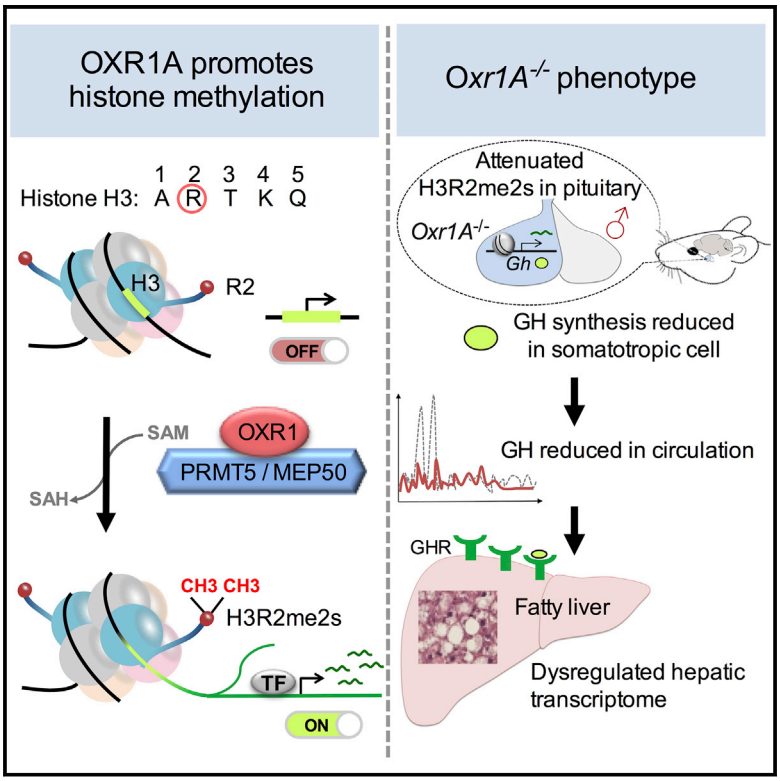

Highlights

- OXR1A interacts with histone arginine methyltransferase PRMT5
- OXR1A stimulates PRMT5/MEP50-mediated H3 methylation *in vitro*
- OXR1A promotes GH expression in pituitary via H3R2 symmetric demethylation
- Depletion of *Oxr1A* results in GH deficiency and fatty liver in adult male mice

Authors

Mingyi Yang, Xiaolin Lin, Filip Segers, ..., Bente Halvorsen, Pål Aukrust, Magnar Bjørås

Correspondence

paukrust@ous-hf.no (P.A.), magnar.bjoras@rr-research.no (M.B.)

In Brief

Yang et al. show that OXR1A interacts with methyltransferase PRMT5 to promote arginine methylation of histone H3R2 and to regulate transcription of growth hormone in the pituitary gland. Male mice with OXR1A knockout display growth-hormone deficiency and develop fatty liver.

Yang et al., 2020, Cell Reports *30*, 4165–4178
March 24, 2020
https://doi.org/10.1016/j.celrep.2020.02.063

CellPress

Cell Reports
Article

OXR1A, a Coactivator of PRMT5 Regulating Histone Arginine Methylation

Mingyi Yang,[1,2,10] Xiaolin Lin,[1,2,10] Filip Segers,[3,10] Rajikala Suganthan,[1] Gunn A. Hildrestrand,[1] Johanne E. Rinholm,[1] Per Arne Aas,[5] Mirta M.L. Sousa,[5,8,9] Sverre Holm,[3] Nils Bolstad,[2] David Warren,[2] Rolf K. Berge,[6,7] Rune F. Johansen,[1] Arne Yndestad,[3] Elise Kristiansen,[1] Arne Klungland,[1] Luisa Luna,[1] Lars Eide,[2] Bente Halvorsen,[3] Pål Aukrust,[3,4,*] and Magnar Bjørås[1,2,5,8,11,*]

[1]Department of Microbiology, Oslo University Hospital, Oslo, Norway
[2]Department of Medical Biochemistry, Oslo University Hospital and University of Oslo, Oslo, Norway
[3]Research Institute of Internal Medicine, Oslo University Hospital and University of Oslo, Oslo, Norway
[4]Section of Clinical Immunology and Infectious Diseases, Oslo University Hospital, Oslo, Norway
[5]Department of Clinical and Molecular Medicine, Norwegian University of Science and Technology, Trondheim, Norway
[6]Department of Clinical Science, University of Bergen, Bergen, Norway
[7]Department of Heart Disease, Haukeland University Hospital, Bergen, Norway
[8]Department of Laboratory Medicine, St. Olavs Hospital, Trondheim, Norway
[9]Proteomics and Metabolomics Core Facility-PROMEC, Norwegian University of Science and Technology, the Central Norway Regional Health Authority, Trondheim, Norway
[10]These authors contributed equally
[11]Lead Contact
*Correspondence: paukrust@ous-hf.no (P.A.), magnar.bjoras@rr-research.no (M.B.)
https://doi.org/10.1016/j.celrep.2020.02.063

SUMMARY

Oxidation resistance gene 1 (*OXR1*) protects cells against oxidative stress. We find that male mice with brain-specific isoform *A* knockout ($Oxr1A^{-/-}$) develop fatty liver. RNA sequencing of male $Oxr1A^{-/-}$ liver indicates decreased growth hormone (GH) signaling, which is known to affect liver metabolism. Indeed, *Gh* expression is reduced in male mice $Oxr1A^{-/-}$ pituitary gland and in rat $Oxr1A^{-/-}$ pituitary adenoma cell-line GH3. $Oxr1A^{-/-}$ male mice show reduced fasting-blood GH levels. Pull-down and proximity ligation assays reveal that OXR1A is associated with arginine methyl transferase PRMT5. OXR1A-depleted GH3 cells show reduced symmetrical dimethylation of histone H3 arginine 2 (H3R2me2s), a product of PRMT5 catalyzed methylation, and chromatin immunoprecipitation (ChIP) of H3R2me2s shows reduced *Gh* promoter enrichment. Finally, we demonstrate with purified proteins that OXR1A stimulates PRMT5/MEP50-catalyzed H3R2me2s. Our data suggest that OXR1A is a coactivator of PRMT5, regulating histone arginine methylation and thereby GH production within the pituitary gland.

INTRODUCTION

The oxidation resistance gene 1 (*OXR1*) is highly conserved in eukaryotes and was originally identified as an anti-oxidation gene in yeast (Elliott and Volkert, 2004; Fischer et al., 2001). This role has been confirmed in several other species, including humans (Yang et al., 2015; Yang et al., 2014), mice (Finelli et al., 2015; Liu et al., 2015; Oliver et al., 2011), worms (Sanada et al., 2014), and insects (Jaramillo-Gutierrez et al., 2010). Mice lacking all OXR1 isoforms displayed severe neurodegeneration and died early after birth (Jaramillo-Gutierrez et al., 2010; Oliver et al., 2011). Recently, studies in mice showed that overexpression of *OXR1* in neurons extends the survival of an amyotrophic lateral sclerosis model, perhaps reflecting the relation of OXR1 to oxidative stress (Liu et al., 2015). Studies in *C. elegans* reveal that *OXR1* has a role in regulating aging and maintaining a normal lifespan (Sanada et al., 2014), but its molecular function and the roles in physiology and pathophysiology are still incompletely understood.

Brain pathology has been shown to induce systemic metabolic alterations, such as those contributing to metabolic syndromes and liver steatosis, potentially involving disturbed signaling of neurotransmitters and hormones including pituitary-gland-derived mediators (e.g., growth hormone [GH] and thyroid stimulating hormone [TSH]) (Auer et al., 2016; Brown et al., 1997; Chishima et al., 2017; Ichikawa et al., 2007; Sos et al., 2011). The regulation and operating molecules of these pathways, including the brain-liver axis, however, are far from clear.

Similar to humans (Elliott and Volkert, 2004; Yang et al., 2014), mice express at least four different *OXR1* isoforms (Fischer et al., 2001). Although all tissues appear to express the shortest isoform, *Oxr1D*, the longest isoform (*Oxr1A*) in mice is expressed only in the brain. Isoform *B* is not expressed in the brain but in other tissues, such as the liver and the heart. We have recently generated a brain-specific *Oxr1A* knockout (KO) mouse model. Based on the putative role of OXR1 as a sensor of cellular oxidative stress (Yang et al., 2014, 2015) and the possible role of these processes in the regulation of neuroendocrine responses, we used OXR1A-deficient mice and *Oxr1A* knockdown and KO cell lines to study the brain-liver axis with a focus on neuroendocrine regulation. We found that $Oxr1A^{-/-}$ mice developed liver steatosis, associated with reduced GH levels and indications

of decreased GH receptor signaling in the liver. Our results further suggest that OXR1A acts as a coactivator of protein arginine methyltransferase 5 (PRMT5), increasing symmetrical dimethylation of histone H3 arginine 2 at the *Gh* promoter in the pituitary gland and, consequently, increases *Gh* transcription. These data reveal a role for OXR1A in oxidative stress signaling as a regulator of protein arginine methylation, which promotes *Gh* expression in the pituitary gland and thereby influences liver lipid metabolism.

RESULTS

Construction of a Brain-Specific *Oxr1A*$^{-/-}$ Mouse Strain

By searching the mice genome databases and comparing them with human *OXR1*, we identified at least six *Oxr1* transcript variants that can be classified into *A*, *B1–B4*, and *D* isoforms (Figures 1A and S1A). Each isoform has one or several unique exons at the 5′ end. The longest isoform, *Oxr1A* (GeneBank: NM_001130166), consists of 17 exons with three unique exons (exons 1–3).

A brain-specific *Oxr1A* KO mouse strain (*Oxr1A*$^{-/-}$) was generated by the gene-trap approach (Figures 1A and S1B). The KO mice were viable and produced offspring normally (Mendelian distribution). The KO genotype was verified by PCR (Figure S1B). Further, western blot analysis with an OXR1A-specific antibody (OXR1 Ab1, made by our laboratory) showed that the OXR1A protein was lacking in the *Oxr1A*$^{-/-}$ brain (Figure 1B). Our previous studies demonstrated that human *OXR1A* is expressed only in the brain (Yang et al., 2014). Similarly, mouse *Oxr1A* also appears to be expressed in the brain, including the pituitary gland in wild-type (WT) (Figure S1C) but not in the liver (Figure 1B). Western blot analysis of the same brain and liver tissues samples as above, using an OXR1 antibody (OXR1 Ab2, Bethyl Laboratories, Inc.), which recognized an epitope mapping to exon 8 in both isoforms (*A* and *B*), confirmed that OXR1A is lacking in the *Oxr1A*$^{-/-}$ brain. In addition, livers of WT and *Oxr1*$^{-/-}$ mice showed the same levels of OXR1B expression, demonstrating that knocking out *Oxr1A* did not affect the protein expression of OXR1B in the liver (Figure 1B). In agreement with the protein data, by using *Oxr1A*-specific primers spanning exons 2–3 (Figure S1A), qPCR analysis showed that *Oxr1A* mRNA was significantly expressed only in the brain of WT, but not in the brain of KO, mice or in the liver or other tissues (i.e., kidney, spleen, testis, lung, and thymus) of both WT and KO mice (Figure S1D). Thus, the *Oxr1A* isoform is selectively expressed in the brain and in the pituitary gland, but not in the liver or any other tissues analyzed.

OXR1A$^{-/-}$ Mice Display Liver Steatosis

Based on the relationship between the brain and systemic metabolic pathways, including the brain-liver axis, we hypothesized that deficiency in *Oxr1A*, with expression restricted to the brain, could induce systemic metabolic disturbances, such as liver steatosis. Indeed, histological examination of the liver of 12-month-old mice showed markedly enhanced fat accumulation in the male *Oxr1A* KO as compared with WT mice (Figure 1C). Further characterization of these mice showed increased hepatic triglyceride levels, but not cholesterol levels, in *Oxr1A*$^{-/-}$, as compared with WT, mice, with the most pronounced changes in the male mice (Figure 1D). These findings demonstrate the development of liver steatosis in *Oxr1A*$^{-/-}$ mice. Twelve-month-old, male KO mice, but not the female, also showed altered oral glucose tolerance, indicating decreased insulin sensitivity (Figure 1E). Moreover, 12-month-old male and female *Oxr1A* KO mice showed a tendency toward increased body weight as compared with WT mice (Figure 1F). In contrast, the body weight was significantly reduced at day 3, 8, and 9 in young *Oxr1A*$^{-/-}$ mice. In addition, *Oxr1A*$^{-/-}$ mice showed a tendency toward reduced body weight gain in the first 3 weeks after birth (Figure S1E). All together, these data suggest that OXR1A is involved in stimulating body growth, and the increase in body weight in 12-month-old KO mice might reflect secondary phenomenon related to disturbed metabolism. To further examine the growth phenotype and liver steatosis, food intake was monitored (Figure S1F), and no differences were observed between the genotypes. To test whether the liver steatosis phenotype was associated with alterations in fatty acid (FA) oxidation and synthesis, we examined the hepatic activity of three enzymes involved in FA oxidation (i.e., carnitine palmitoyl transferase I [CPT-1], CPT-2, and fatty acid oxidase [FAO]), showing no differences between the two genotypes (Figures S1G–S1I). In addition, even when testing sensitivity to the natural key inhibitor of CPT-1, malonyl-coenzyme A (CoA), we found no differences between the two genotypes (Figure S1I), underscoring that there are no differences in hepatic mitochondrial beta-oxidation of FA between WT and *Oxr1A*$^{-/-}$ mice. These findings suggest that the effect of *Oxr1A* KO on liver steatosis is mediated through other mechanisms or through other FA metabolic proteins.

Differentially Expressed Genes (DEGs) of *Oxr1A*$^{-/-}$ Male Liver Are Enriched in Hormone Response, Fatty Liver Metabolism, and Immune Response

To provide mechanistic insight into how the absence of OXR1A in the brain triggers fatty liver, we investigated the transcription profile and compared the DEGs in the liver of 12-month-old mice. The RNA sequencing (RNA-seq) data of mice liver consist of four groups with three biological replicates in each group: WT males, *Oxr1A*$^{-/-}$ males, WT females, and *Oxr1A*$^{-/-}$ females. Principal-component analysis (PCA) showed that the difference in the transcriptomes between *Oxr1A*$^{-/-}$ and WT mice was much larger in males than it was in females (Figure S2A). We identified 724 DEGs in males, and most of them were upregulated in *Oxr1A*$^{-/-}$ mice in comparison to WT mice (652 genes upregulated and 72 genes downregulated). In contrast, only 169 genes (64 upregulated and 105 downregulated) were differentially expressed in the female of *Oxr1A*$^{-/-}$ mice (Figure 2A; Tables S1 and S2). In total, 49 genes are commonly regulated by OXR1A in both genders, whereas a large number of DEGs (675 genes) were uniquely regulated in males (Figure S2B). To verify the liver RNA-seq data, we measured the mRNA level of DEGs by RT-PCR. In agreement with the RNA-seq, all the tested genes showed significant differences in transcription level between WT and OXR1A-deficient mice (Figure S2H). Gene Ontology (GO) analysis showed that, in male mice, a subset of DEGs (22 genes) is enriched in FA metabolism (Figures 2B and 2C), whereas the other three subsets of genes are enriched in

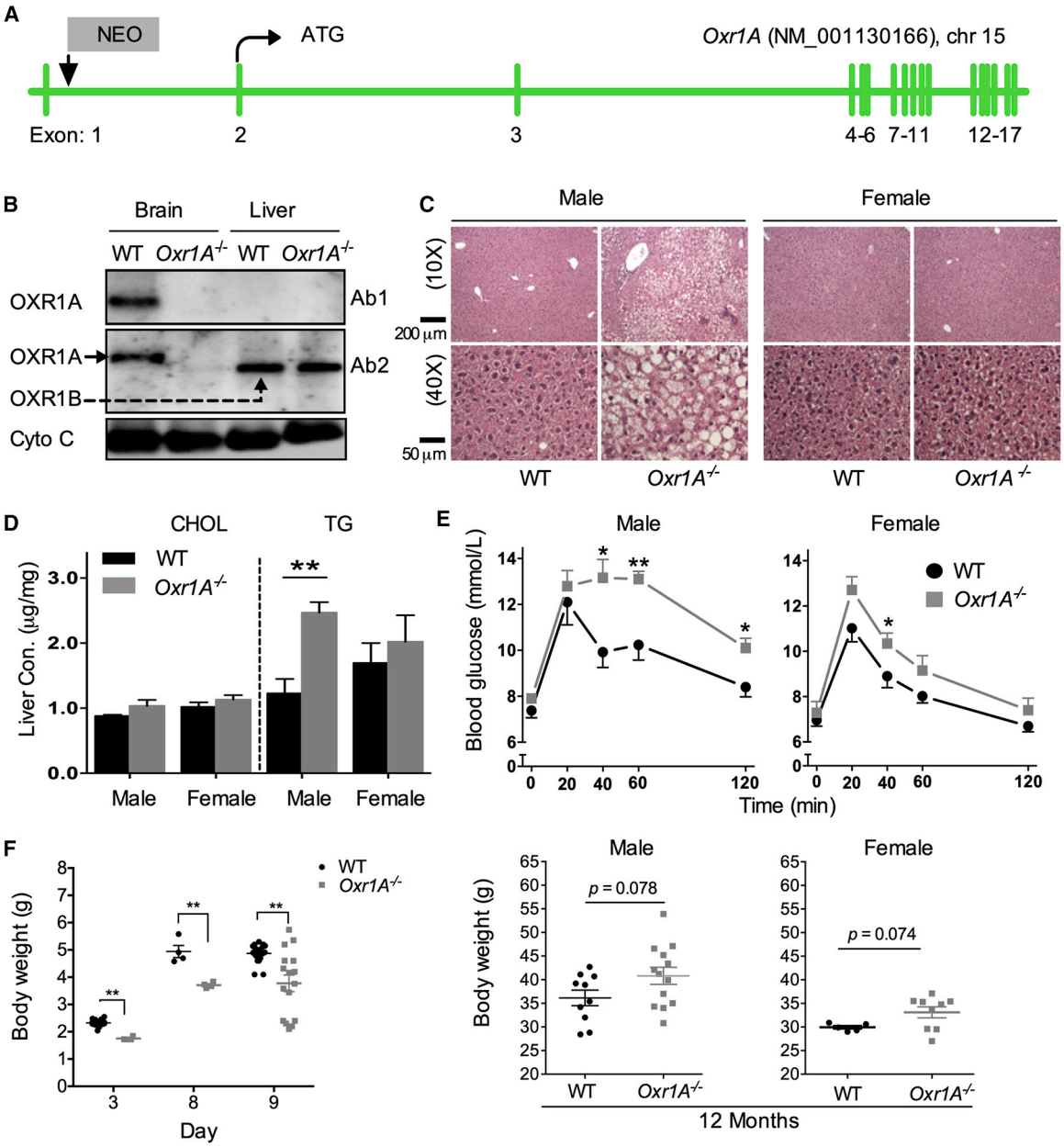

Figure 1. OXR1A Deficiency Causes Fatty Liver in Male Mice

(A) *Oxr1A* knockout (KO) generated by the gene trap approach. A DNA fragment that included the neomycin gene (NEO) and a long terminal repeat sequence was inserted into the intron between exons 1 and 2 to disrupt *Oxr1* transcription.

(B) Verification of *Oxr1A* KO by western blot analysis, using an antibody (Ab1) that specifically recognizes OXR1A or an antibody (Ab2) that recognizes both OXR1A and B proteins. Cytochrome *c* (Cyto C) was used as the loading control.

(C) Hematoxylin and eosin stains of the liver of 12-month-old mice.

(D) Triglyceride (TG) and cholesterol (CHOL) levels in the liver of 12-month-old *Oxr1A*$^{-/-}$ and WT mice. n = 8 (WT, male), 13 (*Oxr1A*$^{-/-}$, male), 5 (WT, female), and 9 (*Oxr1A*$^{-/-}$, female).

(E) Oral glucose tolerance test of 12-month-old mice. n = 7 (WT, male), 11 (*Oxr1A*$^{-/-}$, male), 2 (WT, female), and 5 (*Oxr1A*$^{-/-}$, female).

(F) Body weight of mice.

Error bars represent mean ± SD. *p < 0.05, **p < 0.01.

See Figure S1.

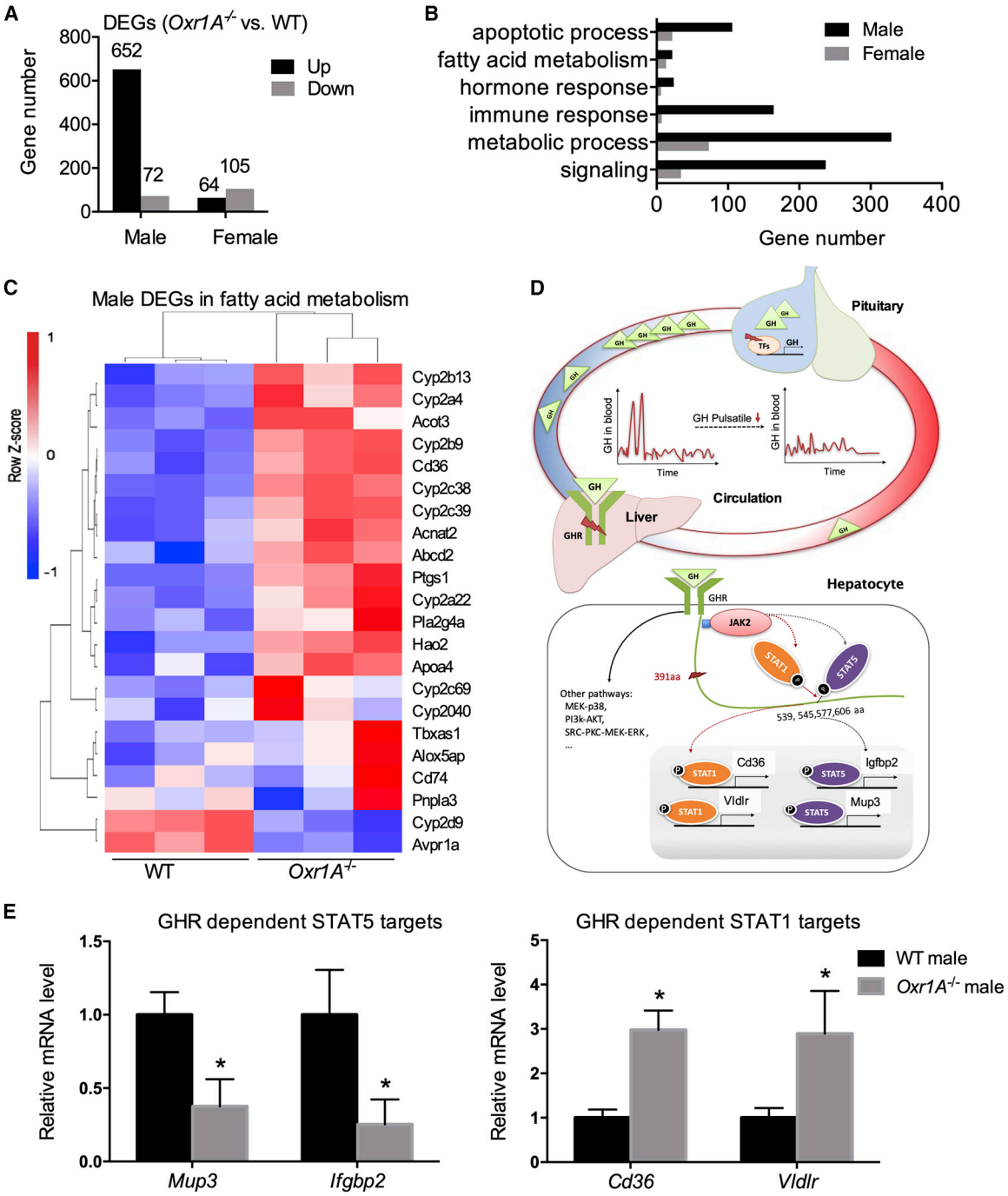

Figure 2. Dysregulation of the Transcriptome in the Liver of OXR1A-Deficient Male Mice

(A) Total numbers of differentially expressed genes (DEGs) in the liver of 12-month-old *Oxr1A*$^{-/-}$ mice as compared with WT.

(B) GO biological process enrichment analysis of DEGs in the livers of 12-month-old *Oxr1A*$^{-/-}$ mice as compared with WT.

(C) Heatmap for a subset of DEGs enriched in fatty acid metabolism and transport in 12-month-old *Oxr1A*$^{-/-}$ male mice as compared with WT controls.

(D) Schematic diagram of GH regulation of hepatocyte transcriptome via the GHR-STAT5 axis. The *Gh* expression is regulated by Pit1 in the pituitary gland and transported to hepatocytes via blood circulation where it binds to the GH receptor (GHR) and induces JAK2-mediated STAT5 phosphorylation. Phosphorylated STAT5 translocates to the nucleus and activates the transcription of its target genes. Inactivation or depletion of GHR or STAT5 results in STAT1 activation (arrow with dash line in red).

(E) Transcription levels of GHR-dependent STAT5- and STAT1-targeted genes in the livers of 12-month-old male mice. The mRNA was measured by qPCR. n = 3. Error bars represent mean ± SD. *p < 0.05.

See Figure S2 and Tables S1, S2, S3, and S4.

the hormone response (24 genes), immune response (164 genes), and apoptosis (106 genes) (Figures 2B and S2E–S2G). The total number of DEGs and enrichment in several steatosis-related processes were much less pronounced in females than they were in males (Figure 2B). GO molecular-function analysis revealed that the major classes of DEGs belonged to binding and catalytic activity (Figure S2C). Kyoto Encyclopedia of Genes and Genomes (KEGG) pathway-enrichment analysis showed that the pathogenesis of this fatty liver disease also involves immune activation, enhanced apoptosis, and abnormal lipid metabolism (Figure S2D). For instance, we observed more than a 2-fold increase in expression of *Il1b* (interleukin-1 beta) in *Oxr1A* KO male mice (Figure S2H).

The pituitary gland secretes several hormones of importance for systemic metabolism, such as GH and TSH. Indeed, both TSH and, in particular, GH deficiency have been related to liver steatosis (Auer et al., 2016; Brown et al., 1997; Chishima et al., 2017; Ichikawa et al., 2007; Sos et al., 2011). *Oxr1A* is expressed in the pituitary gland (Figure S1C). The murine major urinary proteins (Mups) are encoded by at least 21 genes, named *Mup1–21*. The liver Mups are regulated by hormones, including GH, thyroxin, and testosterone. As such, Mups serve as biomarkers for pituitary-gland-related hormones (Knopf et al., 1983). RNA-seq showed that 13 *Mup* genes in male *Oxr1A*$^{-/-}$ mice were significantly downregulated, especially those that are typical for male mice (e.g., *Mup20*, *Mup7*, and *Mup11*) (Figure S2I). In females, 9 *Mup* genes were also downregulated in *Oxr1A*$^{-/-}$ mice, including those that are typical for females (e.g., *Mup4* and *Mup13*) (Figure S2I; Table S1).

The Liver Transcriptome of the GHR-STAT5 Axis-Deficient Male Mice Resembles That of *Oxr1A*$^{-/-}$ Male Mice

Based on our data, we speculated that the liver steatosis in *Oxr1A*$^{-/-}$ mice could be related to downregulation of GH secretions from the pituitary gland. In liver, GH binds to the GH receptor (GHR) in hepatocytes, thereby activating transcription factor STAT5 via JAK2-mediated phosphorylation (Barclay et al., 2011; Zhang et al., 2012) (Figure 2D). Previous studies have demonstrated that most GH-regulated hepatic genes are subject to STAT5 control (Barclay et al., 2010). The kinetics of GHR-JAK-STAT activation, in particular, the activation of STAT5, is critically dependent on the pulse pattern of the GH secretion (Choi and Waxman, 2000; Gebert et al., 1997). Indeed, our RNA-seq data showed that 68 of the total 775 DEGs were targets of STAT5 in *Oxr1A*$^{-/-}$ male liver, indicating that GH-mediated regulation of JAK2-STAT5 activation was altered, which may suggest that the pulsatile secretion pattern of GH is attenuated in OXR1A-deficient male mice. A KEGG pathway enrichment analysis further confirmed that the Jak-STAT pathway was significantly enriched (Table S3). Comparison of the transcriptome of *Oxr1A*$^{-/-}$ male livers with the transcriptomes of the livers of the *Ghr-391* mutant, *Ghr*$^{-/-}$ (Barclay et al., 2011), *Pit1* mutant, or *Prop1*- and *Ghrhr*-mutant mice (Boylston et al., 2006; Swindell, 2007), showed many common DEGs (Table S4). For example, the *Oxr1A*$^{-/-}$ mice showed reduced expression of STAT5 target genes *Igfbp2* and *Mup3* (Table S1; Figure 2E). Moreover, lack of STAT5 activation leads to increased *Stat1* transcription and activation (protein expression and phosphorylation) (Barclay et al., 2011). This is consistent with our findings demonstrating increased expression of *Stat1* and its target genes, including *Cd36* and *Vldlr* (very low density lipoprotein receptor) in *Oxr1A* $^{-/-}$ liver, both of major importance for lipid metabolism and transport within the liver (Figure 2E; Tables S1 and S3). These overlaps in the liver gene-expression profiles further support the involvement of GH deficiency in the induction of liver steatosis in *Oxr1A*$^{-/-}$ male mice.

Reduced GH Level in Blood of *Oxr1A*$^{-/-}$ Male Mice

Our data so far, and in particular the downregulation of 13 *Mup* genes in male *Oxr1A*$^{-/-}$ mice, could suggest the involvement of altered pituitary hormones, such as GH in the liver steatosis seen in *Oxr1A* $^{-/-}$ mice. To further examine our hypothesis, we tested the influence of OXR1A on blood levels of pituitary-derived hormones that could be related to liver steatosis, such as GH, FSH (follicle-stimulating hormone), ACTH (adrenocorticotropic hormone), and TSH. We first measured blood GH levels after 4 h of fasting as a standard test for de-masking GH deficiency. Although fasting dramatically induced GH levels in the blood in 6-month-old WT mice with an average of a 20-fold increase, that result was not seen in *Oxr1A*$^{-/-}$ male mice (Figure 3A). Further, 12-month-old mice showed no significant differences in ACTH, FSH, and TSH levels in blood between the two genotypes (Figure S3A). These data support OXR1A as regulating GH, but not regulating ACTH, FSH, and TSH. IGF-1 (insulin-like growth factor 1) is a well-characterized protein that can be positively regulated by GH. However, the blood IGF-1 level is not reduced in the *Oxr1A* KO male mice as compared with the WT mice (Figure S3B).

Gene Expressions of *Gh* in the Pituitary Gland Are Reduced in *Oxr1A*$^{-/-}$ Male Mice

Our findings so far suggest that GH deficiency could mediate the liver phenotype in *Oxr1A*$^{-/-}$ mice. Therefore, we next performed a series of experiments to examine how OXR1A could regulate GH. Western blot analysis showed that OXR1A was indeed expressed in the pituitary gland, as well as in the whole brain of WT, but not *Oxr1A*$^{-/-}$, mice (Figures 1B and S1C). Next, we examined the gene expression of *Gh* (Figure 3B) in pituitary glands of 6-month-old *Oxr1A*$^{-/-}$ and WT mice. Although the gene-expression levels of *Gh* were spread over a large range in the pituitary gland of 6-month-old WT mice, showing a 5-fold difference between the lowest and the highest value, *Gh* expression in the *Oxr1A*$^{-/-}$ pituitary gland showed no variation because all mice displayed values similar to the lowest values in WT mice. Thus, it appears that WT mice express *Gh* over a dynamic range in 6-month-old pituitary glands, in support of a pulsatile expression pattern, whereas that regulation is absent in the OXR1A-deficient mice. In the pituitary glands of 12-month-old mice, expression of *Gh* declined to a level below the level at 6 months in both WT and *Oxr1*$^{-/-}$ mice (Figure 3B), indicating that the age-related drop in *Gh* expression accelerated in OXR1A-deficient mice. In fact, the lack of the pulsatile pattern, as well as an impaired response to fasting, is a more reliable feature of GH deficiency than the actual level. In contrast to *Gh*, transcript levels of *Tshb* and *Pomc*, both with potential

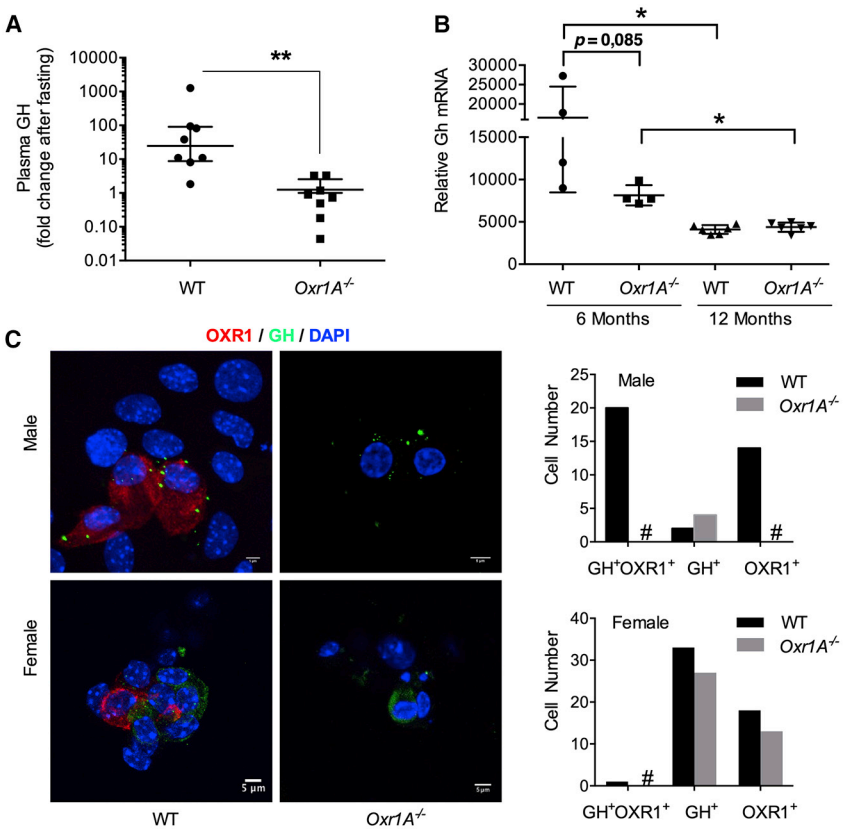

Figure 3. Hormone Expression and Secretion Are Reduced in the Pituitary and Blood, Respectively, in *Oxr1A*$^{-/-}$ Male Mice

(A) The plasma GH protein was measured by ELISA kit in 6-month-old male mice after fasting.

(B) The *Gh* expression in the pituitary of male mice was measured by qPCR. n = 4–6.

(C) Immune staining of OXR1A and GH protein in primary cell cultures derived from the pituitary gland of mice. The numbers of GH-positive (GH$^+$), OXR1A-positive (OXR1$^+$), and double-positive (GH$^+$ OXR1A$^+$) cells were quantified (right panels). At least five fields were counted from each group. #The cell type was not observed.

Error bars represent mean ± SD. *p < 0.05, **p < 0.01. See Figure S3.

relevance for the development of fatty liver, as well as the expressions of several hormone receptors (*Ghrhr*, *Sstr*, *Igf1r*, and *Trhr*) were not differentially regulated in *Oxr1A* KO mice (Figure S3C). Prolactin (*Prl*), however, showed a tendency toward downregulation in 6-month-old *Oxr1A*$^{-/-}$ mice (Figure S6A).

OXR1A Showed the Highest Expression in Primary GH-Producing Pituitary Gland Cells Derived from Male, but Not Female, Mice

To gain further insight in the function of OXR1 in the regulation of GH expression, we generated primary cell cultures derived from the anterior lobe of the murine pituitary gland. Fluorescence microscopy with anti-GH showed that a minor sub-population of the cells was GH positive (Figure 3C). Notably, staining of cultures derived from male mice showed that OXR1A was enriched in GH-producing cells. In female-derived cultures, OXR1A-positive cells showed no significant GH staining, whereas GH-positive cells lacked OXR1 staining (Figure 3C). Thus, it appears that OXR1A-mediated regulation of *Gh* expression is sex dependent, supporting the theory that dysregulation of hepatic GH signaling and fatty liver occurs predominantly in male *Oxr1A*$^{-/-}$ mice.

GH-Producing Cells Co-expressed OXR1A in Male Pituitary Gland

The overall size of the pituitary glands from adult WT and *Oxr1A*$^{-/-}$ male mice was similar (Figure S3E). To evaluate the histological characteristics of the pituitary glands in more detail, we performed histological analysis on the whole pituitary gland from adult male mice. H&E staining (Figure S3F) showed no obvious differences in morphology between the KO and control mice. Both genotypes displayed similar well-developed structures consisting of three lobes: anterior, posterior, and intermediate pituitary. GH-producing cells made up the main part of the anterior lobe.

Similar to the results from the primary cultured pituitary cells, staining of tissue sections with an anti-OXR1A antibody showed that OXR1A was more enriched in GH-producing cells in males than it was in females. About 50% (51/100) of GH-producing cells co-expressed OXR1A in the male pituitary, whereas only 25% (22/89) in the female (Figure S3G).

To explore the location of OXR1A in relation to other hormone-producing cells in the pituitary gland, we performed a series of immunofluorescence staining with anterior pituitary glands from both adult male and female WT mice. We found OXR1A co-expressed with part of the LH- and TSH-producing cells in both adult male and female mice, with part of the PRL-producing cells in female. There was little co-localization of OXR1 in ACTH- and FSH-producing cells in both male and female mice. (Figure S3H).

PRMT5 Interacts with OXR1 in Cell Extracts

To reveal the molecular function of OXR1A underlying regulation of *Gh* expression, we searched for protein interaction partners of OXR1. We generated U2OS cell lines with stable expression of human OXR1A-GFP or GFP alone that were used in immunoprecipitation (IP) experiments with anti-GFP. The proteins pulled down from the IP were analyzed by mass spectrometry (MS). Of particular interest, we found that the protein arginine methyltransferase 5 (PRMT5) precipitated together with OXR1A (Table S5). This IP experiment was repeated three times, and we detected PRMT5 every time in the pull-down fraction by MS. Control experiments repeated three times with the GFP protein alone showed no detectable pull-down of PRMT5.

To further map the domain involved in the interaction with PRMT5, we performed a similar coimmunoprecipitation (coIP)

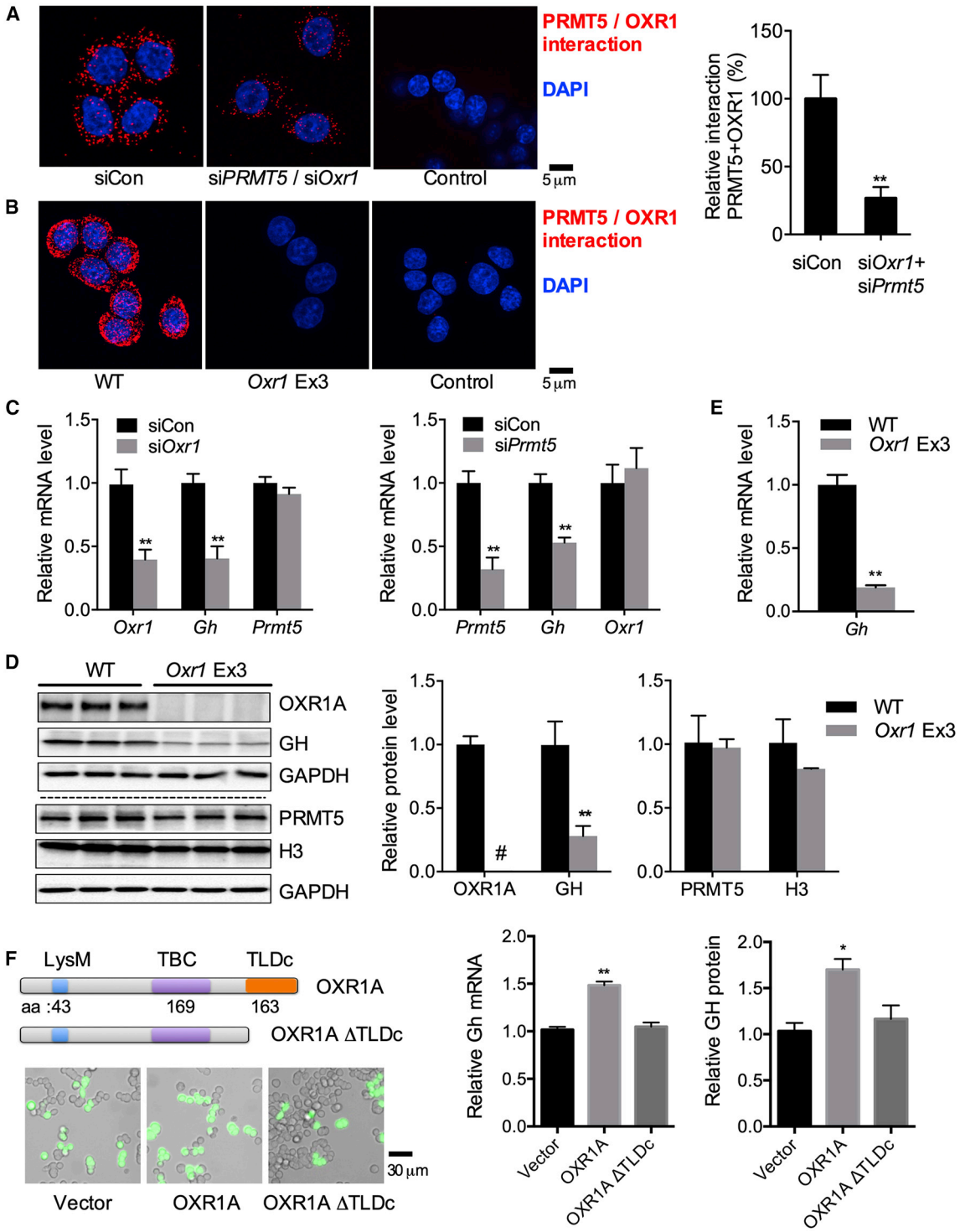

Figure 4. OXR1 Interacts with PRMT5 to Promote *Gh* Expression in Rat Pituitary Cell Line GH3

(A and B) A proximity ligation assay was performed to detect the interaction between OXR1A and PRMT5 (red spots) in GH3 cells with or without si*Prmt5* and si*Oxr1* knockdown (A) or in WT and *Oxr1A*$^{-/-}$ GH3 cells (B). The nuclei were stained with DAPI. The interaction was detected with both OXR1 and PRMT5 antibodies. OXR1 antibody alone (A) or PRMT alone (B) showed no signal (negative control). The interaction was quantified (right panel) as the percentage of the signal intensity related to that of the control (siCon) in (A). At least 30 cells were analyzed from each group.

(C) *Gh* expression was measured in GH3 cells transfected by control siRNA (siCon), si*Oxr1*, or si*Prmt5*. Three days after siRNA transfection, total RNA was isolated, and the *Gh* expression was measured by qPCR. *Actin* was used as the internal control. n = 4.

(legend continued on next page)

with U2OS cells overexpressing OXR1D-GFP. Notably, PRMT5 was also identified as one of the OXR1D-binding proteins. The OXR1D isoform mainly consists of the TLDc domain presented in all OXR1 isoforms, thus suggesting that the TLDc domain may facilitate the interaction between OXR1 and PRMT5. PRMT5 has been shown to form complexes with MEP50 (methylosome protein 50, encoded by gene *WDR77*) to catalyze protein arginine methylation (Antonysamy et al., 2012; Blanc and Richard, 2017; Stopa et al., 2015). However, MEP50 was not significantly enriched by coIP in U2OS cells of the overexpression OXR1A or OXR1D. One possibility is that MEP50 is below detection level. To increase sensitivity in detecting potential OXR1 protein partners, we performed targeted MS of coIP proteins. Indeed, we found that some known protein partners of PRMT5, such as MEP50, ICLN, and WDR5, co-purified with OXR1A as well as OXR1D, supporting the idea that the core domain of OXR1 (the TLDc domain) facilitates these protein interactions (Figures S4A–S4G).

Verification of the OXR1 and PRMT5 Interaction *In Vivo*

The PRMT5 has a crucial role in regulation of many intracellular processes, including transcription by symmetric dimethylation of arginine on histones H2A, H3, and H4 or non-histone proteins (Berger, 2008; Burgos et al., 2015; Chen et al., 2017; Chu et al., 2015; Guo et al., 2010; Jansson et al., 2008; Kim et al., 2014; Scoumanne et al., 2009; Stopa et al., 2015; Yang and Bedford, 2013). To verify the interaction of endogenous OXR1A with PRMT5, we performed proximity ligation assays (PLAs) in a rat pituitary adenoma-derived cell line GH3 (Figures 4A and 4B). The PLA showed strong signals for OXR1A-PRMT5 interactions both in cytoplasm and the nucleus in control small interfering RNA (siRNA)-transfected cells, whereas cells transfected with si*Oxr1* and si*Prmt5* showed a strong reduction in signal intensity. There was no detectable signal in PLA control assays using only one primary antibody (i.e., anti-OXR1A) in control siRNA-transfected cells (Figure 4A). Thus, it appears that, in pituitary cells, OXR1A interacts with PRMT5. Western blot analysis confirmed that the GH3 cells transfected with si*Oxr1* and si*Prmt5* showed reduced expression of the siRNA-targeted proteins (Figure S5A). Next, we generated GH3 *Oxr1A* KO cell lines by the CRISPR-Cas9 approach (Shalem et al., 2014) targeting exon 3 (*Oxr1* Ex3). Consistent with the siRNA data above, the PLA interaction signals between OXR1A and PRMT5 were strong in both the cytoplasm and the nucleus of WT cells but totally lost in GH3 *Oxr1A* KO cells (Figure 4B), confirming that isoform OXR1A interacts with PRMT5. These data are clearly demonstrating that OXR1A and PRMT5 interact both in the nucleus and the cytoplasm *in vivo*.

In addition, fluorescence microscopy of primary mouse pituitary cell cultures showed co-localization between OXR1A and PRMT5 mainly in the cytoplasm but also in the nucleus (Figure S5B). Finally, we examined the interaction between purified recombinant PRMT5 and OXR1A by surface plasmon resonance (Biacore). We were not able to detect any significant interaction between purified OXR1A and PRMT5 (data not shown), which may indicate that the interaction is weak in the absence of protein partners present in the cell, such as other PRMT5-interacting partners (i.e., MEP50, ICLN, and WDR5) shown to be present in pull-down experiments with OXR1A or OXRD (Figure S4A–S4G). In contrast, histone H3.1 was not enriched by pull-down with OXR1A or OXR1D (Figure S4H).

In addition to PRMT5, PRMT1 also interacts with *Oxr1A*$^{-/-}$. PRMT1 functionally catalyzes monomethylation and asymmetric dimethylation at arginine sites on histones and other proteins. PLAs using OXR1A and PRMT1 antibodies showed strong signals in GH3 cells transfected with control siRNA, whereas the signals were strongly reduced in si*Oxr1* and si*Prmt1* double-knockdown GH3 cells (Figure S5C). Western analysis confirmed that si*Prmt1* knockdown reduced its protein expression efficiently (Figure S5A). The targeted MS also detected PRMT1 in the pull-down from OXR1A and OXR1D (Figure S4). Overall, these data strongly suggest that OXR1A interacts directly with PRMT1 and PRMT5 within the pituitary gland.

OXR1A and PRMT5 Regulate *Gh* Expression in Pituitary Gland Cell Line GH3

To examine the role of OXR1A and PRMT5 in transcriptional regulation of *Gh*, we measured the mRNA levels of *Gh* in the rat GH3 cell line by qPCR. In RNAi experiments, expression of *Gh* was significantly reduced after silencing *Oxr1* (targeting all isoforms) or *Prmt5* (Figure 4C). The expression level of *Gh* was reduced 60% in *Oxr1*-silenced cells as compared with control cells. These data may suggest that the interaction of OXR1 and PRMT5 has a role in transcriptional regulation of *Gh*. Next, we used the GH3 *Oxr1A* KO cell line targeting exon 3 to examine *Gh* expression. Western analysis showed that the OXR1A protein was absent in the KO strain (Figure 4D). Notably, GH protein and *Gh* gene expression decreased 80% and 90%, respectively, as compared with WT controls (Figure 4D). Similarly, KO of *Oxr1* with guide RNA targeting exon 5 (which is unique for isoform *A* and *B*) or exon 15 (a common exon for all isoforms), also resulted in reduction in GH protein expression (Figure S5D). Pulsatility and gender dimorphism in GH secretion is regulated by GHRH (growth hormone releasing hormone) and SST (somatostatin) produced in hypothalamus. To explore whether OXR1A affects GH expression via this axis, we measured gene expression of *Sst* and other related regulators *Igf1*, *Igf1r*, *Ghrh*, *Sstr*, and *Trh*

(D) Western blot analysis. GH levels in *Oxr1A*$^{-/-}$ cells (*Oxr1* Ex3) were calculated relative to that of WT cells. Glyceraldehyde-3-phosphate dehydrogenase (GAPDH) was used as loading control. n = 3. #Less than a detectable level.
(E) Gene expression of *Gh* was measured by qPCR. n = 3.
(F) GH gene and protein expression were significantly increased in OXR1A-KO GH3 cells rescued by full-length human OXR1A, but not by a mutant protein lacking the C-terminal TLDc domain (OXR1A ΔTLDc). Top left: illustration of OXR1A fragments inserted into plasmid pEGFP-N. Bottom left: GH3 OXR1A KO cells 2 weeks after plasmids transfection. Right: *Gh* gene expression was measured by qPCR (n = 6), and GH protein expression was measured by western blot (n = 3). Error bars represent mean ± SD. **$p < 0.01$, *$p < 0.05$.
See Figures S4 and S5 and Tables S5, S6, S7, and S8.

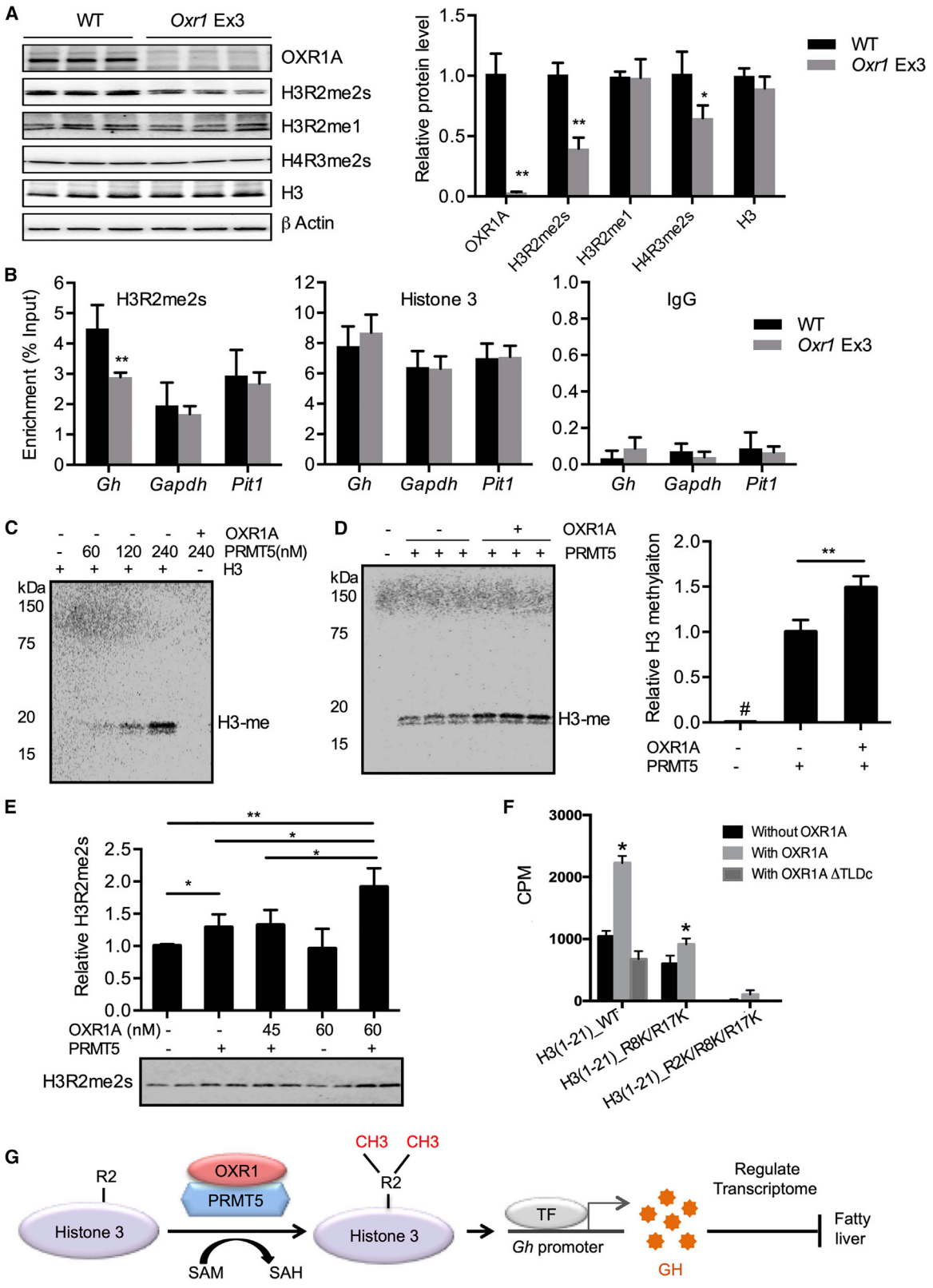

(legend on next page)

in the male hypothalamus (Figure S3D). There were no differences in those genes between the two genotypes, excluding the possibility of OXR1-mediated GH expression via cross talking with hypothalamus regulators.

Forskolin (FSK) induces *Gh* expression in pituitary glands by modulating cellular cyclic AMP (cAMP) concentration and activation of its signaling pathway, including phosphorylation of CREB, which is a key transcription factor upregulating Pit1 expression. Pit1 is a crucial transcription factor for regulating GH expression (Monteserin-Garcia et al., 2013; Shepard et al., 1994). In agreement with previous reports (Cuttler et al., 1993; Szabo et al., 1990), both *Gh* and *Prl* expressions were increased after treatment with 5 μM of FSK for 3 h. Importantly, FSK-induced GH was attenuated by *Oxr1A* knockdown (Figure S5E). Interestingly, FSK also induced *Oxr1* expression. Thus, FSK-induced Gh expression is at least partly dependent on OXR1 and is correlated with upregulation of OXR1 in transcription.

To test whether PRMT5 cooperates with OXR1 in Gh regulation, we silenced *Prmt5* in *Oxr1A* KO GH3 cells. The data showed no further significant reduction of *Gh* expression as compared with the *Oxr1A* KO control, suggesting that PRMT5 and OXR1 operate via the same pathway/mechanism for *Gh* regulation (Figure S5F). All together, these data strongly suggest that *Gh* transcription in the pituitary gland is regulated by OXR1A and PRMT5.

Transcriptome Analyses of the Pituitary Gland Cell Line GH3 Show a Role for OXR1A in Regulation of GH and Signal Transduction

To further examine the role of OXR1A in transcription regulation in the pituitary, we performed RNA-seq of three biological replicates of OXR1A KO and WT GH3 cell lines. We identified 484 DEGs; of which, 352 genes were downregulated and 132 genes were upregulated in OXR1A KO GH3 cells in comparison to WT controls (Figure S5G). RNA-seq showed that *Gh* gene expression was significantly downregulated in OXR1A KO cells (Figure S5H), which is consistent with the qPCR results (Figure 4E). Analysis using the KEGG database showed that the top enriched pathways of the DEGs contained cAMP signaling, focal adhesion, MAPK signaling, and extracellular matrix (ECM)-receptor interaction, indicating OXR1A has an important role in cellular signaling transduction via transcription regulation (Table S6). In addition, GO analysis showed that the cellular components of the DEGs were enriched in extracellular regions (Table S7), whereas the molecular functions were mainly enriched in protein binding, cytokine activity, and ion channel activity (Table S8). In sum, GH3 RNA-seq supports a role for OXR1A in transcription regulation in the pituitary gland, including GH expression and signal transduction.

The C-Terminal TLDc Domain in OXR1A Is Crucial for Regulation of *Gh* Expression

To map the functional effect of the core TLDc domain of OXR1A in transcription regulation of GH, we performed rescue experiments in GH3 OXR1A KO cells by expressing full-length human OXR1A (hOXR1A) and hOXR1A lacking the C-terminal TLDc domain (OXR1A ΔTLDc) (Figure 4F). Both proteins were fused to GFP in the pEGFP-N vector, showing 30%–40% transfection efficiency (Figure 4F). Notably, GH expression of both mRNA and the protein levels in GH3 OXR1 KO cells were significantly rescued by full-length hOXR1A but not by the truncated hOXR1A protein-expressed cells. These results suggest that the C-terminal TLDc domain is crucial for regulation of *Gh* expression. Accordingly, expression by the hOXR1A full-length protein showed significant increase of the H3R2me2s modification in GH3 KO cells (Figure S5I).

OXR1 Promotes Symmetric Dimethylation of Histone H3 Arginine 2 at the *Gh* Promoter

PRMT5 is the primary methyltransferase for symmetric dimethylation of arginine *in vivo*. Of particular importance for transcriptional activation, PRMT5 dimethylates histone H3 arginine 2

Figure 5. OXR1 Promotes Histone Arginine Methylation *In Vivo* and *In Vitro*

(A) Western blot analysis of PRMT5 catalyzed histone H3 methylation in WT (WT) and *Oxr1A*$^{-/-}$ GH3 cells (*Oxr1* Ex3). Methylated H3 in *Oxr1A*$^{-/-}$ was calculated relative to that of WT cells. H3R2me2s, H3R2 symmetric dimethylation; H3R2me1, H3R2 monomethylation; H4R3me2s, H4R3 symmetric dimethylation. Actin was used as loading control. n = 3.

(B) ChIP assay with the H3R2me2s or H3 antibody. IgG was used as a negative control. Enrichment of promoters of genes was quantified by qPCR and is presented as a percentage related to chromatin input. n = 4.

(C) C^{14} SAM-based H3 methylation assay with PRMT5 or OXR1A. The reactions were supplied with H3 (22 μM) and increasing concentrations PRMT5/MEP50 (60–240 nM). Control experiments were performed with PRMT5/MEP50 (240 nM) and/or OXR1A (600 nM) without H3 (last lane). H3-me, methylated H3.

(D) C^{14} SAM-based H3 methylation assay with PRMT5 and OXR1A together. The reaction was supplied with H3 (22 μM), PRMT5/MEP50 complex (120 nM), and OXR1A (600 nM). Left panel: one representative experiment. Right panel: quantification of H3 methylation from two experiments. n = 6. #Signal was not detectable.

(E) The H3R2me2s-specific antibody was used to detect arginine-specific methylation on H3 by western blot. The reactions were supplied with the PRMT5/MEP50 complex (15 nM) and two concentrations of OXR1A (45 and 60 nM). Bottom panel: one representative experiment. Top panel: quantification from two experiments. n = 6.

(F) Methylation assays with N-terminal H3 peptides as the substrate and PRMT5 and full-length OXR1A or OXR1A lacking 163 aa at the C-terminal end (OXR1A ΔTLDc). WT and two mutant N-terminal H3 peptides (aa 1–21) were used as substrates: H3 (1–21)_WT, H3 (1–21)_R8K/R17K, and H3 (1–21)_R2K/R8K/R17K. The reactions were supplied with PRMT5/MEP50 complex in presence of [^{3}H] SAM. Methylated peptides were detected by scintillation counting. Representative data presented from one of two independent quadruplicate assays. Error bars represent SD. *p < 0.05, compared with its relative setting without OXR1A.

(G) Model of OXR1A function and mechanism of action. OXR1A-PRMT5-dependent symmetric dimethylations of histone H3 arginine 2 (H3R2me2s) on the *GH* promoter activate gene expression. Consequently, depletion of OXR1A results in reduced *Gh* expression, dysregulation of liver metabolism, and fatty liver disease.

Error bars represent mean ± SD. *p < 0.05, **p < 0.01.

See Figure S6.

symmetrically (H3R2me2s) to maintain euchromatin (Migliori et al., 2012). Further, H3R2me2s promotes H3K4 trimethylation and downstream gene activation (Kirmizis et al., 2007; Yuan et al., 2012). Therefore, we hypothesized that OXR1A promotes PRMT5-dependent H3R2me2s and facilitates transcription of *Gh*. First, we measured the cellular level of H3R2me2s and other PRMT5-catalyzed histone modifications in GH3 cells. Western blot analysis showed that H3R2me2s and H4R3me2s were reduced 60% and 20%, respectively, in *Oxr1A*$^{-/-}$ cells as compared with WT cells (Figure 5A). H3R2 monomethylation (H3R2me1) was not significantly changed in OXR1A-deficient cells (Figure 5A). Next, we examined enrichment of H3R2me2s at the *Gh* promoter by chromatin immunoprecipitation (ChIP) from *Oxr1A*$^{-/-}$ and WT GH3 cells. Indeed, the *Oxr1A*$^{-/-}$ GH3 cell line showed reduced H3R2me2s binding to the *Gh* promoters but no reduction of binding to *Gapdh* and *Pit1* promoters as compared with WT cells (Figure 5B). The enrichment of the *Gh* promoter shown by ChIP with the H3R2me2s antibody in WT cells was more than 100-fold greater than the ChIP with only immunoglobulin G (IgG) (Figure 5B), confirming the specificity of the H3R2me2s antibody. ChIP with the histone H3 antibody showed the same enrichment of *Gh* promoters in *Oxr1A*$^{-/-}$ and WT cells, demonstrating that the reduction of H3R2me2s is not caused by a reduction in histone H3 on the *Gh* promoters. In agreement with those results, knockdown of *Oxr1* in GH3 cells by siRNA showed a reduction in enrichment of H3R2me2s at the *Gh* promoter (Figure S6E). In sum, these data suggest that OXR1 regulates *Gh* transcription by promoting PRMT5-catalyzed symmetric dimethylation of histone H3R2. Interestingly, *Prl*, which is regulated by the same transcription factor as *Gh*, Pit1, was also downregulated by knockdown of *Oxr1* and *Prmt5* as well as by KO of *Oxr1A* in GH3 cells (Figure S6B and S6C). ChIP qPCR suggested OXR1 regulates PRL by a mechanism similar to Gh regulation by promoting the H3R2me2s at the *Prl* promoter (Figure S6D).

Recombinant OXR1A Protein Stimulates PRMT5-Catalyzed Symmetric Dimethylation of H3R2 *In Vitro*, Revealing an Essential Role for the C-Terminal TLDc Domain

PRMT5 is reported to associate with methylome protein 50 (MEP50), which has an important role in PRMT5 substrate recognition and catalysis. The PRMT5/MEP50 complex catalyzes both monomethylation and symmetric dimethylation of H3 at R2 (Wang et al., 2014), which is more active than that of PRMT5 alone. Therefore, we used the PRMT5/MEP50 complex in methylation assays with histone H3 as substrate. We employed three methods to detect H3 methylation. First, we monitored the total H3 methylation with ^{14}C *S*-adenosyl-L-methionine (SAM) as methyl donor, showing a linear increase in H3 methylation with increasing concentrations of PRMT5/MEP50 (Figure 5C). Next, we compared methylation of H3 by PRMT5/MEP50 with or without OXR1A purified by Ni-NTA and gel filtration columns (Figure S6F), showing a 1.5-fold increase in H3 methylation in the presence of OXR1A (Figure 5D). In addition, we showed that OXR1A was not methylated by the PRMT5/MEP50 complex (Figure 5C, last lane). These data demonstrated that OXR1A stimulates PRMT5 activity.

Next, we used the histone methylation-specific antibodies to measure H3R2 monomethylation (H3R2me1) and symmetric dimethylation (H3R2me2s). The PRMT5/MEP50 complex alone catalyzed symmetrical dimethylation of H3 at a slow rate (Figure 5E). Addition of OXR1A to the reaction mixture with PRMT5/MEP50 stimulated H3R2me2s about 2–3-fold as compared with PRMT5/MEP50 alone (Figures 5E and S6G). We also compared symmetric dimethylation versus monomethylation of H3R2 in parallel with increasing concentrations of OXR1A, suggesting that H3R2me2s is the major product of OXR1 stimulation of PRMT5. (Figure S6G). OXR1 itself did not catalyze H3 dimethylation if the reaction system was lacking PRMT5/MEP50 (Figure 5E).

PRMT5 can methylate several arginine residues at the H3 N-terminal tails, i.e., R2, R8, and R17. To confirm the specificity of OXR1A-dependent co-activation of PRMT5-catalyzed H3R2 methylation, we tested PRMT5/MEP50 methyltransferase activity on WT and mutant peptides of the H3 N-terminal tail (aa 1–21) as substrates. Further, we addressed the role of the C-terminal TLDc domain for PRMT5 co-activation with a truncated version of human OXR1A lacking 163 residues at the C-terminal end (the entire TLDc domain). Methyltransferase assays with PRMT5/MEP50 and H3 (1–21) peptides showed a 2-fold increase in activity by addition of the full-length hOXR1A, whereas OXR1A ΔTLDc showed no significant increase in activity (Figure 5F), strongly suggesting that the C-terminal TLDc domain is essential for co-activation. Control experiments with the H3 (1–21) R2K/R8K/R17K mutant peptide lacking all three R residues showed no activity, demonstrating that the PRMT5 reaction is arginine specific. Moreover, PRMT5 methyltransferase assays with the H3 (1–21) R8K/R17K mutant peptide with only R2 present showed a robust methyltransferase activity, although stimulation by hOXR1A was less proficient but still significant. Taken together, these data indicate that OXR1A is a cofactor for PRMT5/MEP50-mediated symmetric dimethylation at H3R2.

DISCUSSION

The PRMT family targets not only histones but also a number of other cellular proteins. Thus, PRMT5 has a pivotal role in diverse processes, such as transcription, replication, repair, RNA splicing, signaling, cell cycles, differentiation, apoptosis, and tumorigenesis. We show that OXR1A stimulates PRMT5 activity *in vitro*, and depletion of OXR1A reduced H3R2me2s *in vivo*. Thus, OXR1A is possibly involved in a wide range of biological processes via interaction with PRMTs. For example, PRMT5 is reported to directly methylate tumor suppressor p53, which is a transcription factor regulating the expression of genes involved in cell cycle arrest and apoptosis in response to DNA damage (Jansson et al., 2008). Our previous study showed that siRNA-mediated OXR1 depletion led to cell cycle arrest in G2/M, and differential expression in a subset of p53-regulated genes under oxidative stress (Yang et al., 2015). A recent study demonstrated that murine OXR1 binds with PRMT1 *in vitro* using immunoprecipitation (Finelli et al., 2015). This interaction is suggested to promote the relocalization of FUS and Tdp-43 to the nucleus, avoiding their aggregation in cytoplasm, a characteristic of several neurodegenerative disorders including amyotrophic

lateral sclerosis. Here, we confirm that OXR1A also interacts with PRMT1 in both the nucleus and the cytoplasm (Figure S4C), although the *Oxr1A* KO did not affect the level of H4R3me2a (Figure S6H), which is one of the main histone modification substrates of PRMT1. Thus, whereas OXR1A regulates GH in the pituitary gland through interaction with PRMT5, we may speculate that OXR1A could be a coactivator of several members of the PRMT family, implicating a broader and more general role for OXR1A in regulating cellular processes in response to stress via protein arginine methylation.

Functional mapping of the interaction domain by rescue experiments *in vivo* and biochemical assays with purified recombinant full-length and truncated human OXR1A proteins, suggest a crucial role of the C-terminal TLDc domain in GH regulation and stimulation of PRMT5 activity. Moreover, PLAs verified the physical interaction between endogenous OXR1 and PRMT5 in both the cytoplasm and the nucleus in GH3. In addition to abolishing its role in regulating GH expression *in vivo* (Figure 4F), the OXR1A ΔTLDc mutant showed no stimulation of PRMT5-catalyzed H3R2me2s *in vitro* (Figure 5F). Moreover, we have demonstrated that the OXR1D protein, which basically is composed of the TLDc domain, is interacting with the PRMT5 complex as well.

Although OXR1A is selectively expressed in the brain, *Oxr1A*$^{-/-}$ mice showed features of liver steatosis with high levels of triglycerides within the liver. Several lines of indirect evidence suggest that this was mediated by decreased GH level. First, transcriptome analyses of the liver showed that several of the DEGs are enriched in hormone-regulated pathways. Second, male *Oxr1A*$^{-/-}$ mice display reduced liver expression of *Mup* genes, which are pituitary gland hormone-responsive genes. Third, Oxr1A$^{-/-}$ male mice showed markedly attenuated GH response to fasting. In contrast, no differences were seen in TSH, FSH, and ACTH levels in blood, and transcriptional levels of these pituitary-derived hormones were not altered in *Oxr1A*$^{-/-}$ male mice.

Finally, we have uncovered a molecular function of OXR1A as a coactivator of PRMT5 that activates gene transcription of *Gh* via histone arginine methylation in the pituitary gland (Figure 5G). As such, OXR1 may provide a new drug target for manipulating GH levels and preventing metabolic diseases in human.

STAR★METHODS

Detailed methods are provided in the online version of this paper and include the following:

- KEY RESOURCES TABLE
- LEAD CONTACT AND MATERIALS AVAILABILITY
- EXPERIMENTAL MODEL AND SUBJECT DETAILS
  - *In Vivo* Experiments
- METHOD DETAILS
  - Tissue Preparation
  - Nucleic acid isolation and quantification
  - RNA sequencing
  - Gene expression by Quantitative Real-Time Polymerase Chain Reaction
  - Western blot and antibodies
  - Proximity ligation assay
  - Primary pituitary cell culture
  - Plasmids
  - Mass spectrometry for identification of OXR1A interaction partners
  - Targeted mass spectrometry
  - Immunofluorescent staining
  - Isotope C^{14} SAM based methylation assay
  - Antibody-based methylation assay
  - Methylation assays with H3 N-terminal tail (aa 1-21) peptides
  - Generation of rat OXR1 knockout cell line
  - Mouse GH ELISA assay
  - Chromatin immunoprecipitation (CHIP)
  - Histological staining in liver tissues
  - Hepatic triglyceride (TG) and cholesterol (CHOL) measurements
  - Activities of murine liver enzymes involved in FA metabolism
  - Oral Glucose Tolerance Test and Blood glucose measurement
- QUANTIFICATION AND STATISTICAL ANALYSIS
- DATA AND CODE AVAILABILITY

SUPPLEMENTAL INFORMATION

Supplemental Information can be found online at https://doi.org/10.1016/j.celrep.2020.02.063.

ACKNOWLEDGMENTS

Fluorescence microscopy was performed with support from Dr. Jens Eriksson and Stig Ove Bøe at the South-East Health Authority Core Facility of Advanced Light Microscopy (Gaustad, Norway). Protein mass spectrometry was performed with support from Dr. Gustavo Souza at the South-East Health Authority Core Facility of Proteomics (Gaustad, Norway). The study was supported by grants from the South-East Health Authority (grants 2014092 and 2017117), the Norwegian Cancer Society (grant 182744-2016), and The Research Council of Norway (grants 240099/F20, 24973, and 239211).

AUTHOR CONTRIBUTIONS

M.Y., X.L., F.S., A.Y., B.H., L.E., P.A., and M.B. planned all experiments, analyzed the data, and wrote the paper; M.Y., X.L., F.S., R.S., G.A.H., J.E.R., P.A.A., M.M.L.S., S.H., N.B., R.K.B., R.F.J., and E.K. performed all experiments; and D.W., A.K., and L.L. provided advice on data analyses and the manuscript.

DECLARATION OF INTERESTS

The authors declare no competing interests.

Received: September 18, 2017
Revised: January 4, 2020
Accepted: February 13, 2020
Published: March 24, 2020

REFERENCES

Antonysamy, S., Bonday, Z., Campbell, R.M., Doyle, B., Druzina, Z., Gheyi, T., Han, B., Jungheim, L.N., Qian, Y., Rauch, C., et al. (2012). Crystal structure of the human PRMT5:MEP50 complex. Proc. Natl. Acad. Sci. USA *109*, 17960–17965.

Auer, M.K., Stalla, G.K., and Stieg, M.R. (2016). Investigating the role of cortisol and growth hormone in fatty liver development: fatty liver index in patients with pituitary adenomas. Pituitary *19*, 461–471.

Barclay, J.L., Kerr, L.M., Arthur, L., Rowland, J.E., Nelson, C.N., Ishikawa, M., d'Aniello, E.M., White, M., Noakes, P.G., and Waters, M.J. (2010). In vivo targeting of the growth hormone receptor (GHR) Box1 sequence demonstrates that the GHR does not signal exclusively through JAK2. Mol. Endocrinol. *24*, 204–217.

Barclay, J.L., Nelson, C.N., Ishikawa, M., Murray, L.A., Kerr, L.M., McPhee, T.R., Powell, E.E., and Waters, M.J. (2011). GH-dependent STAT5 signaling plays an important role in hepatic lipid metabolism. Endocrinology *152*, 181–192.

Berger, S.L. (2008). Out of the jaws of death: PRMT5 steers p53. Nat. Cell Biol. *10*, 1389–1390.

Blanc, R.S., and Richard, S. (2017). Arginine methylation: the coming of age. Mol. Cell *65*, 8–24.

Boylston, W.H., DeFord, J.H., and Papaconstantinou, J. (2006). Identification of longevity-associated genes in long-lived Snell and Ames dwarf mice. Age (Dordr.) *28*, 125–144.

Brown, S.B., Maloney, M., and Kinlaw, W.B. (1997). "Spot 14" protein functions at the pretranslational level in the regulation of hepatic metabolism by thyroid hormone and glucose. J. Biol. Chem. *272*, 2163–2166.

Burgos, E.S., Wilczek, C., Onikubo, T., Bonanno, J.B., Jansong, J., Reimer, U., and Shechter, D. (2015). Histone H2A and H4 N-terminal tails are positioned by the MEP50 WD repeat protein for efficient methylation by the PRMT5 arginine methyltransferase. J. Biol. Chem. *290*, 9674–9689.

Chen, H., Lorton, B., Gupta, V., and Shechter, D. (2017). A TGFβ-PRMT5-MEP50 axis regulates cancer cell invasion through histone H3 and H4 arginine methylation coupled transcriptional activation and repression. Oncogene *36*, 373–386.

Chishima, S., Kogiso, T., Matsushita, N., Hashimoto, E., and Tokushige, K. (2017). The relationship between the growth hormone/insulin-like growth factor system and the histological features of nonalcoholic fatty liver disease. Intern. Med. *56*, 473–480.

Choi, H.K., and Waxman, D.J. (2000). Pulsatility of growth hormone (GH) signalling in liver cells: role of the JAK-STAT5b pathway in GH action. Growth Horm. IGF Res. *10* (*Suppl B*), S1–S8.

Chu, Z., Niu, B., Zhu, H., He, X., Bai, C., Li, G., and Hua, J. (2015). PRMT5 enhances generation of induced pluripotent stem cells from dairy goat embryonic fibroblasts via down-regulation of p53. Cell Prolif. *48*, 29–38.

Cuttler, L., Collins, B.J., Marone, P.A., and Szabo, M. (1993). The effect of isobutylmethylxanthine, forskolin, and cholera toxin on growth hormone release from pituitary cell cultures of perinatal and mature rats. Endocr. Res. *19*, 33–46.

Elliott, N.A., and Volkert, M.R. (2004). Stress induction and mitochondrial localization of Oxr1 proteins in yeast and humans. Mol. Cell. Biol. *24*, 3180–3187.

Fauskanger, M., Haabeth, O.A.W., Skjeldal, F.M., Bogen, B., and Tveita, A.A. (2018). Tumor killing by $CD4^+$ T cells is mediated *via* induction of inducible nitric oxide synthase-dependent macrophage cytotoxicity. Front. Immunol. *9*, 1684.

Finelli, M.J., Liu, K.X., Wu, Y., Oliver, P.L., and Davies, K.E. (2015). Oxr1 improves pathogenic cellular features of ALS-associated FUS and TDP-43 mutations. Hum. Mol. Genet. *24*, 3529–3544.

Fischer, H., Zhang, X.U., O'Brien, K.P., Kylsten, P., and Engvall, E. (2001). C7, a novel nucleolar protein, is the mouse homologue of the *Drosophila* late puff product L82 and an isoform of human OXR1. Biochem. Biophys. Res. Commun. *281*, 795–803.

Gebert, C.A., Park, S.H., and Waxman, D.J. (1997). Regulation of signal transducer and activator of transcription (STAT) 5b activation by the temporal pattern of growth hormone stimulation. Mol. Endocrinol. *11*, 400–414.

Guo, Z., Zheng, L., Xu, H., Dai, H., Zhou, M., Pascua, M.R., Chen, Q.M., and Shen, B. (2010). Methylation of FEN1 suppresses nearby phosphorylation and facilitates PCNA binding. Nat. Chem. Biol. *6*, 766–773.

Hsu, P.D., Scott, D.A., Weinstein, J.A., Ran, F.A., Konermann, S., Agarwala, V., Li, Y., Fine, E.J., Wu, X., Shalem, O., et al. (2013). DNA targeting specificity of RNA-guided Cas9 nucleases. Nat. Biotechnol. *31*, 827–832.

Ichikawa, T., Nakao, K., Hamasaki, K., Furukawa, R., Tsuruta, S., Ueda, Y., Taura, N., Shibata, H., Fujimoto, M., Toriyama, K., and Eguchi, K. (2007). Role of growth hormone, insulin-like growth factor 1 and insulin-like growth factor-binding protein 3 in development of non-alcoholic fatty liver disease. Hepatol. Int. *1*, 287–294.

Jain, K., Jin, C.Y., and Clarke, S.G. (2017). Epigenetic control via allosteric regulation of mammalian protein arginine methyltransferases. Proc. Natl. Acad. Sci. USA *114*, 10101–10106.

Jansson, M., Durant, S.T., Cho, E.C., Sheahan, S., Edelmann, M., Kessler, B., and La Thangue, N.B. (2008). Arginine methylation regulates the p53 response. Nat. Cell Biol. *10*, 1431–1439.

Jaramillo-Gutierrez, G., Molina-Cruz, A., Kumar, S., and Barillas-Mury, C. (2010). The *Anopheles gambiae* oxidation resistance 1 (OXR1) gene regulates expression of enzymes that detoxify reactive oxygen species. PLoS ONE *5*, e11168.

Kim, S., Günesdogan, U., Zylicz, J.J., Hackett, J.A., Cougot, D., Bao, S., Lee, C., Dietmann, S., Allen, G.E., Sengupta, R., and Surani, M.A. (2014). PRMT5 protects genomic integrity during global DNA demethylation in primordial germ cells and preimplantation embryos. Mol. Cell *56*, 564–579.

Kim, D., Langmead, B., and Salzberg, S.L. (2015). HISAT: a fast spliced aligner with low memory requirements. Nat. Methods *12*, 357–360.

Kirmizis, A., Santos-Rosa, H., Penkett, C.J., Singer, M.A., Vermeulen, M., Mann, M., Bähler, J., Green, R.D., and Kouzarides, T. (2007). Arginine methylation at histone H3R2 controls deposition of H3K4 trimethylation. Nature *449*, 928–932.

Knopf, J.L., Gallagher, J.F., and Held, W.A. (1983). Differential, multihormonal regulation of the mouse major urinary protein gene family in the liver. Mol. Cell. Biol. *3*, 2232–2240.

Liu, K.X., Edwards, B., Lee, S., Finelli, M.J., Davies, B., Davies, K.E., and Oliver, P.L. (2015). Neuron-specific antioxidant OXR1 extends survival of a mouse model of amyotrophic lateral sclerosis. Brain *138*, 1167–1181.

MacLean, B., Tomazela, D.M., Shulman, N., Chambers, M., Finney, G.L., Frewen, B., Kern, R., Tabb, D.L., Liebler, D.C., and MacCoss, M.J. (2010). Skyline: an open source document editor for creating and analyzing targeted proteomics experiments. Bioinformatics *26*, 966–968.

Migliori, V., Müller, J., Phalke, S., Low, D., Bezzi, M., Mok, W.C., Sahu, S.K., Gunaratne, J., Capasso, P., Bassi, C., et al. (2012). Symmetric dimethylation of H3R2 is a newly identified histone mark that supports euchromatin maintenance. Nat. Struct. Mol. Biol. *19*, 136–144.

Monteserin-Garcia, J., Al-Massadi, O., Seoane, L.M., Alvarez, C.V., Shan, B., Stalla, J., Paez-Pereda, M., Casanueva, F.F., Stalla, G.K., and Theodoropoulou, M. (2013). Sirt1 inhibits the transcription factor CREB to regulate pituitary growth hormone synthesis. FASEB J. *27*, 1561–1571.

Øie, E., Berge, R.K., Ueland, T., Dahl, C.P., Edvardsen, T., Beitnes, J.O., Bohov, P., Aukrust, P., and Yndestad, A. (2013). Tetradecylthioacetic acid increases fat metabolism and improves cardiac function in experimental heart failure. Lipids *48*, 139–154.

Oliver, P.L., Finelli, M.J., Edwards, B., Bitoun, E., Butts, D.L., Becker, E.B., Cheeseman, M.T., Davies, B., and Davies, K.E. (2011). Oxr1 is essential for protection against oxidative stress-induced neurodegeneration. PLoS Genet. *7*, e1002338.

Sanada, Y., Asai, S., Ikemoto, A., Moriwaki, T., Nakamura, N., Miyaji, M., and Zhang-Akiyama, Q.M. (2014). Oxidation resistance 1 is essential for protection against oxidative stress and participates in the regulation of aging in Caenorhabditis elegans. Free Radic. Res. *48*, 919–928.

Scoumanne, A., Zhang, J., and Chen, X. (2009). PRMT5 is required for cell-cycle progression and p53 tumor suppressor function. Nucleic Acids Res. *37*, 4965–4976.

Shalem, O., Sanjana, N.E., Hartenian, E., Shi, X., Scott, D.A., Mikkelson, T., Heckl, D., Ebert, B.L., Root, D.E., Doench, J.G., and Zhang, F. (2014).

Genome-scale CRISPR-Cas9 knockout screening in human cells. Science *343*, 84–87.

Shepard, A.R., Zhang, W., and Eberhardt, N.L. (1994). Two CGTCA motifs and a GHF1/Pit1 binding site mediate cAMP-dependent protein kinase A regulation of human growth hormone gene expression in rat anterior pituitary GC cells. J. Biol. Chem. *269*, 1804–1814.

Sos, B.C., Harris, C., Nordstrom, S.M., Tran, J.L., Balázs, M., Caplazi, P., Febbraio, M., Applegate, M.A., Wagner, K.U., and Weiss, E.J. (2011). Abrogation of growth hormone secretion rescues fatty liver in mice with hepatocyte-specific deletion of JAK2. J. Clin. Invest. *121*, 1412–1423.

Spears, M., Taylor, K.J., Munro, A.F., Cunningham, C.A., Mallon, E.A., Twelves, C.J., Cameron, D.A., Thomas, J., and Bartlett, J.M. (2012). In situ detection of HER2:HER2 and HER2:HER3 protein-protein interactions demonstrates prognostic significance in early breast cancer. Breast Cancer Res. Treat. *132*, 463–470.

Stopa, N., Krebs, J.E., and Shechter, D. (2015). The PRMT5 arginine methyltransferase: many roles in development, cancer and beyond. Cell. Mol. Life Sci. *72*, 2041–2059.

Swindell, W.R. (2007). Gene expression profiling of long-lived dwarf mice: longevity-associated genes and relationships with diet, gender and aging. BMC Genomics *8*, 353.

Szabo, M., Staib, N.E., Collins, B.J., and Cuttler, L. (1990). Biphasic action of forskolin on growth hormone and prolactin secretion by rat anterior pituitary cells in vitro. Endocrinology *127*, 1811–1817.

Tarazona, S., García-Alcalde, F., Dopazo, J., Ferrer, A., and Conesa, A. (2011). Differential expression in RNA-seq: a matter of depth. Genome Res. *21*, 2213–2223.

Vakili, H., Jin, Y., Nagy, J.I., and Cattini, P.A. (2011). Transgenic mice expressing the human growth hormone gene provide a model system to study human growth hormone synthesis and secretion in non-tumor-derived pituitary cells: differential effects of dexamethasone and thyroid hormone. Mol. Cell. Endocrinol. *345*, 48–57.

Wang, M., Fuhrmann, J., and Thompson, P.R. (2014). Protein arginine methyltransferase 5 catalyzes substrate dimethylation in a distributive fashion. Biochemistry *53*, 7884–7892.

Yang, Y., and Bedford, M.T. (2013). Protein arginine methyltransferases and cancer. Nat. Rev. Cancer *13*, 37–50.

Yang, M., Luna, L., Sørbø, J.G., Alseth, I., Johansen, R.F., Backe, P.H., Danbolt, N.C., Eide, L., and Bjørås, M. (2014). Human OXR1 maintains mitochondrial DNA integrity and counteracts hydrogen peroxide-induced oxidative stress by regulating antioxidant pathways involving p21. Free Radic. Biol. Med. *77*, 41–48.

Yang, M., Lin, X., Rowe, A., Rognes, T., Eide, L., and Bjørås, M. (2015). Transcriptome analysis of human OXR1 depleted cells reveals its role in regulating the p53 signaling pathway. Sci. Rep. *5*, 17409.

Yuan, C.C., Matthews, A.G., Jin, Y., Chen, C.F., Chapman, B.A., Ohsumi, T.K., Glass, K.C., Kutateladze, T.G., Borowsky, M.L., Struhl, K., and Oettinger, M.A. (2012). Histone H3R2 symmetric dimethylation and histone H3K4 trimethylation are tightly correlated in eukaryotic genomes. Cell Rep. *1*, 83–90.

Zhang, Y., Laz, E.V., and Waxman, D.J. (2012). Dynamic, sex-differential STAT5 and BCL6 binding to sex-biased, growth hormone-regulated genes in adult mouse liver. Mol. Cell. Biol. *32*, 880–896.

STAR★METHODS

KEY RESOURCES TABLE

REAGENT or RESOURCE	SOURCE	IDENTIFIER
Antibodies		
anti-Actin β (AC-15)	Santa Cruz	Cat# sc-69879; RRID:AB_1119529
anti-Growth hormone antibody	R&D system	Cat# AF1566; RRID:AB_354865
anti-GAPDH-HRP	Abcam	Cat# ab9482; RRID:AB_307272
anti-Histone H3 antibody - Nuclear Loading Control and ChIP Grad	Abcam	Cat# ab1791; RRID:AB_302613
anti-Histone H3 (mono methyl R2) antibody - ChIP Grade	Abcam	Cat# ab15584; RRID:AB_880446
anti-Histone H3R2 Symmetric Dimethyl Polyclonal Antibody	Epigentek	Cat# A-3705-100; RRID:AB_2313773
Anti-Histone H4 (symmetric di methyl R3) antibody - ChIP Grade	Abcam	Cat# ab5823; RRID:AB_10562795
anti-OXR1 Ab1	Made by NB and DW in our labs.	Cat# N106.1; RRID:AB_2313773
anti-OXR1 Ab2	Bethyl Laboratories	Cat# A302-035A; RRID:AB_1576567
anti-PRMT1	cell signaling	Cat# 2449; RRID:AB_2237696
anti-PRMT5	GeneTex	Cat# GT3610; Cat# MA5-31465; RRID:AB_2787097
anti-PRMT5	cell signaling	Cat# 2252; RRID:AB_10694541
IgG-HRP anti-goat	Santa Cruz	Cat# sc-2768; RRID:AB_656964
IgG-HRP anti-mouse	SIGMA	Cat# A9044; RRID:AB_258431
IgG-HRP anti-rabbit	Abcam	Cat# ab6721; AB_955447)
Anti-Rabbit IgG–Cy3 antibody produced in sheep	SIGMA	Cat# C2306; RRID:AB_258792
Donkey anti-Goat IgG (H+L) Cross-Adsorbed Secondary Antibody, Alexa Fluor 488	Thermo Fisher	Cat# A-11055; RRID:AB_2534102
Alexa Fluor® 488 Goat Anti-Rabbit IgG (H+L) Antibody	Life/Invitrogen	Cat# A-11034; RRID:AB_2576217
Alexa Fluor® 594 Goat Anti-Mouse IgG (H+L) Antibody	Life/Invitrogen	Cat# A-11005; RRID:AB_141372
Bacterial and Virus Strains		
E.coli competent Cells ER2566	Our Lab.	N/A
E.coli competent Cells BL21-CodonPlus (DE3)-RILP	Agilent	Cat#230280
Trans-lentiviral packaging Mix	Thermo Scientific	TLP4606
Chemicals, Peptides, and Recombinant Proteins		
S-adenosylmethionine (SAM)	New England Biolabs	Cat# B9003S
Formaldehyde solution	Sigma	Cat# F8775
trypsin inhibitor	Sigma	Cat3 T6522
Collagenase type I	Sigma Aldrich	Cat# C0130
Pancreatin	Sigma Aldrich	Cat#P7545
Hyaluronidase	Sigma Aldrich	Cat# H3506
hematoxylin	Vector Laboratories	Cat# H-3502
eosin	Histolab	Cat# 01650
Puromycin	Invitrogen	Cat# A1113802
Recombinant PRMT5 complex	Active motif	Cat#31356

(*Continued on next page*)

Continued

REAGENT or RESOURCE	SOURCE	IDENTIFIER
Recombinant Histone H3 (C110A)	Active motif	Cat#31207
Calf H3	Sigma Aldrich	Cat#11034758001
OXR1A protein	Our Lab.	Human OXR1A
Peptide H3(1-21)_WT	GenScript	Cat# SC1208
Peptide H3(1-21)_R8K/R17K	GenScript	Cat# SC1634
Peptide H3(1-21)_R2K/R8K/R17K	GenScript	Cat# SC1208
Critical Commercial Assays		
Proximity ligation assay kit: Duolink® *In Situ* Red Starter Kit Mouse/Rabbit	Sigma	Cat#DUO92101
methyl transferase assay: isotope [^{14}C]SAM (Adenosyl -L-Methionine, S-[methyl-14C])	Perkin Elmer	Cat#NEC363010UC
Chromatin extraction kit	Abcam	Cat# Ab117152
ChIP Kit Magnetic - One Step	Abcam	Cat#ab156907
Rat/Mouse Growth Hormone ELISA	Merck Millipore	Cat#EZRMGH-45
X-tremeGENE HP DNA Transfection Reagent	Roche	Cat# 6366236001
Lab Assay Cholesterol	Wako Chemical GmbH	Cat# 294-65801
Lab Assay Triglyceride	Wako Chemical GmbH	Cat#290-63701
IP assay kit: GFP-Trap M kit	Chromotek	Cat#gtm-20
Deposited Data		
RNA-seq Raw and analyzed data	This paper	GEO: GSE97024
Experimental Models: Cell Lines		
Rat: GH3 WT	ATCC	Cat#CCL-82.1
GH3 Oxr1A −/−	Our Lab.	Oxr1 Ex3
GH3 Oxr1−/−	Our Lab.	Oxr1 Ex15A1
GH3 Oxr1−/−	Our Lab.	Oxr1 Ex5A1
HEK293T	ATCC	Cat#CRL-11268
Human: U2OS	ATCC	Cat#40345
Experimental Models: Organisms/Strains		
Mouse: C57BL/6, wild type	Our Lab.	N/A
Mouse: C57BL/6, Oxr1A knockout	This paper	N/A
Oligonucleotides		
See Table S9 for oligonucleotide information		N.A
Recombinant DNA		
Plasmid: pEGFP-N-OXR1A	This paper	N/A
Plasmid: pEGFP-N-OXR1A ΔTLDc	GeneScript	U6764DE300_15
Plasmid: pET28b-OXR1A	This paper	N/A
Plasmid: pET28b-OXR1A ΔTLDc	GeneScript	U6764DE300_5
Vector: LentiCRISPER V2	Addgene	#52961
Software and Algorithms		
TopHat2	N/A	https://ccb.jhu.edu/software/tophat/index.shtml
DEGseq R package	N/A	https://www.bioconductor.org/packages/release/bioc/html/DEGseq.html
GOseq	N/A	http://bioinf.wehi.edu.au/software/goseq/
Qlucore Omics Explorer 3.0	Qlucore AB, Lund, Sweden	https://www.qlucore.com

LEAD CONTACT AND MATERIALS AVAILABILITY

Further information and requests for resources and reagents should be directed to and will be fulfilled by the Lead Contact, Prof. Magnar Bjorås (Magnar.Bjoras@rr-research.no). All stable reagents generated in this study are available from the Lead Contact with a completed Materials Transfer Agreement.

EXPERIMENTAL MODEL AND SUBJECT DETAILS

In Vivo Experiments

C57BL/6 mice (WT) and C57BL/6 OXR1A knockout mice (*Oxr1A* $^{-/-}$) were bred in-house. The C57BL/6 ES cell clone (IST13330B9) for *Oxr1A* knockout was purchased from Texas A&M institute for Genomic Medicine (TIGM). In brief, the ES cells were injected into Albino C57BL/6 blastocysts, which were transferred to pseudo-pregnant foster mothers to make chimeric mice. F1 mice were generated by breeding male chimeras with C57BL/6 females and F2 homozygous mutant mice were produced by intercrossing F1 homozygous males and females. Genotypes were determined by PCR analysis with DNA samples extracted from mice ears. All mice (male and female at age up to 24 months) were housed in a climate-controlled environment on a 12h light/dark cycle with free access to rodent food and water. Animals were housed in accordance with the laws and regulations controlling experimental procedures in Norway and the European Union's Directive 86/609/EEC.

METHOD DETAILS

Tissue Preparation

Mice were sacrificed by cervical dislocation. The brain was removed and one hemisphere was harvested separating six different regions (cortex, cerebellum, pituitary, thalamus, hypothalamus and hippocampus). All tissue samples were stored in RNAlater (Sigma) at 4°C overnight and then snap-frozen at −80°C for subsequent analysis including protein extraction and nucleic acid isolation. While the other hemisphere was fixed in buffered, 4% paraformaldehyde (PFA) for paraffin-embedding and immunohistochemistry.

Nucleic acid isolation and quantification

Total DNA and total RNA were isolated from sub-regions of the brain using the AllPrep DNA/RNA/Protein Mini Kit (QIAGEN) according to the manufacturer's instructions. Nucleic acid quality and concentration were estimated by Epoch Microplate Spectrophotometer (Bio-Tek).

RNA sequencing

The mRNA was separated from total RNA by Oligo(dT) magnetic beads, and cDNA synthesized by reverse transcription with N6 primer. Adaptors were ligated to the sticky 3′ end of the cDNA. Two specific primers were used in PCR to amplify the ligation products. Denature the PCR product by heating and the single strand DNA is cyclized by splint oligo and DNA ligase. Performed sequencing of the prepared library with SE50 instrument by Beijing Genomics Institute (BGI), China. Primary sequencing data (raw reads) was subjected to quality control (QC) and filtered into clean reads, which were aligned to the reference sequences using *Bowtie2* and mapped to reference mouse genome mm10 using *HISAT* (Kim et al., 2015). The alignment data was utilized to calculate distribution of reads on reference genes and mapping ratio. FPKM, short for Fragments Per Kilobase of transcript per Million mapped reads, was used to calculate the expression level of the gene.

The NOISeqBIO method (Tarazona et al., 2011) was used to screen differentially expressed genes (DEGs) between two groups. This method models the noise distribution in each group of biological replicates from the actual data, and thus maintains good True Positive and False Positive rates when comparing to other methods. The DEGs are determined by the default criteria: Fold-change $\geq$ 2 and diverge probability (P) $\geq$ 0.8. Gene Ontology (GO) and KEGG pathway enrichment analysis were performed using a hypergeometric distribution model with corrected p value $\leq$ 0.05 as a threshold.

Gene expression by Quantitative Real-Time Polymerase Chain Reaction

Two-steps qPCR method was used to determine RNA levels. First, the cDNA was generated from total RNA samples using the High-capacity cDNA reverse transcription kit from Applied Biosystem. Real-time PCR reactions were prepared using Power SYBR Green Kit including about 3 ng cDNA in each reaction, and PCR was performed in the StepOnePlus™ Real-Time PCR System (Applied Biosystem) with the standard cycle conditions: 95°C for 10 min; 40 cycles at 94°C for 15 s and 65°C for 30 s. Samples were measured in triplicates. Gapdh and or Actinß were used as internal standard as indicated. The expression level was calculated by the Cycle Threshold (CT) parameter using the formula: $(^{Probe}CT) - (^{Standard}CT) = z$; Probeexpr = 2^{-z}. A standard curve was generated to confirm that the PCR reactions were run in the linear range. See Table S9 for primer information.

Western blot and antibodies

For western blotting, the brain tissues were homogenized by Fast-pre-24 instrument with setting at 5 kR/S for 30 s. Then added RIPA buffer (150 mM NaCl, 50 mM Tris pH 7.5, 1mM EDTA, 0.1% SDS, 0.5% Sodium deoxycholate, and 1% Triton X-100), and

homogenized again by Fast-pre-24 as above setting and centrifuged at 13000 RPM 15 min at 4°C. The protein was isolated from sub-regions of the brain alternatively using the AllPrep DNA/RNA/Protein Mini Kit (QIAGEN) according to the manufacturer's instructions. Total protein concentrations of the extracts were determined using a BCA-assay (Pierce, division of Thermo Fisher Scientific, USA). The soluble protein extracts were separated by 4%–15% SDS-PAGE (4%–15% Mini PROTEAN TGX, BIO-RAD) and transferred on a PVDF membrane (Trans-blot Turbo mini Format 0.2 uM PVDF, cat.170-4156 by BIO-RAD) using a BioRad Trans-blot instrument. The membrane was blocked with 5% milk or 5% fetal bovine serum (FBS) in PBS-T buffer (137mM NaCl, 2.7mM KCl, 4.3mM Na_2PO_4, 1.4mM KH_2PO_4, 0.1% Tween-20) overnight at 4°C following incubation with the indicated primary antibody overnight at 4°C, washed 3 times with PBS-T buffer. Then the detection antibodies were used. After washing 3 times with PBS-T buffer, the membrane was incubated with ECL substrate (Supersignal west femto, VWR) and the signal was detected by a BIO-RAD Fluorescent Imager and analyzed by Image Lab software. The antibodies used were anti-Actin β (AC-15) (1:5000), anti-Growth hormone antibody (1:2000), anti-GAPDH-HRP (1:5000), anti-Histone H3 antibody (1:1000), anti-Histone H3 (mono methyl R2) antibody (1:300), anti-Histone H3R2 Symmetric Dimethyl Polyclonal Antibody (1:1000), Anti-Histone H4 (symmetric di methyl R3) antibody (1:1000), anti-OXR1 Ab1 (1:2000), anti-OXR1 Ab2 (1:1000), anti-PRMT1 (1:1000), anti-PRMT5 (cell signaling #2252, 1:1000), anti-PRMT5 (GT3610, 1:1000), IgG-HRP anti-goat (1:10000), IgG-HRP anti-mouse (1:10000), IgG-HRP anti-rabbit (1:30000).

Proximity ligation assay

Proximity ligation assays (PLAs) were performed on both fixed siRNA transfected GH3 cells and Oxr1A or total Oxr1 knockout GH3 cell lines. GH3 cell lines were grown on glass coverslips, fixed with 4% PFA (added 1M glycine in the second wash step after fixation), and permeabilized with 0.1% Triton-X/1X PBS. The PLA was conducted according to the manufacturer's instructions using the Duolink® *In Situ* Red Starter Kit Mouse/Rabbit (Cat. No. DUO92101, SIGMA). After blocking for 30 min at 37°C, the cells were incubated with OXR1 (1:200) and PRMT5 antibodies (1:200) overnight at 4°C. PLA Anti-Rabbit PLUS and Anti-Mouse MINUS probes (containing the secondary antibodies conjugated with oligonucleotides, were added and incubated at 37°C for ligation 30 min. Further the fluorescently labeled oligonucleotides resulting in red fluorescence signals were added to the reaction and incubated for amplification at 37°C for 100 min in the dark. The slides were mounted with Duolink® *In Situ* Mounting Medium with DAPI (Cat. No. DUO82040, SIGMA). Microscopy was carried out using a Leica SP8 confocal microscope equipped with × 40 oil immersion lens. The same input parameters were used throughout all experiments. The number of *in situ* PLA signals per cell was quantified using the ImageJ software (NIH). *In situ* PLA signals were counted by enhancing point-like signals and defining a true signal as a local intensity maximum above a background threshold as previously described (Spears et al., 2012).

Primary pituitary cell culture

Anterior pituitary cells of the wild-type and *Oxr1A*$^{-/-}$ mice were dispersed as described previously (Vakili et al., 2011) with some modifications. Wild-type and Oxr1A$^{-/-}$ mice were euthanized by cervical dislocation and anterior pituitary glands were isolated and washed gently with calcium-free phosphate buffered saline (PBS) with 0.1% bovine serum albumin (0.1% BSA/PBS) twice, then chopped in approximately 1 mm^3 pieces with a scalpel and washed again. The tissue fragments were treated with 0.5 mL 0.1% BSA/PBS containing collagenase type I (1 mg/ml, Sigma Aldrich, C0130), pancreatin (0.5 mg/ml, Sigma Aldrich, P7545), hyaluronidase (1 mg/ml, Sigma Aldrich, H3506), and trypsin inhibitor (0.5 mg/ml, Sigma Aldrich, T6522) for 30 min at 37°C on a shaker. The cell suspension was collected in a 15 mL tube and added to 2 mL of FBS. The digestion of the tissue fragments was repeated two times. Digestion was continued by adding 15 units of DNase I (sigma Aldrich, AMPD1) per 5 mL of digested supernatant, with gentle mixing for 2 min at room temperature. The cell suspension was filtered through a nylon mesh and centrifuged for 5 min at 1200 rpm at room temperature. Cells were then suspended, plated at 1 × 10^5 cells/well in 24-well plates with coverslip (VWR ECN631-1577), in Dulbecco's Modified Eagle's Medium (DMEM) including 4.5% glucose (Sigma, D6429) supplemented with 10% (v/v) FBS, antibiotics (100 UI/ml penicillin, 100 μg/ml streptomycin). The cells were cultured at 37°C for 72 h in a humidified atmosphere of 5% CO_2. Hereafter, the cells received fresh medium every 48 h.

Plasmids

The cDNA of human OXR1A ORF (NM_001198533) and the truncated variant of OXR1A lacking the TLDc domain (OXR1A ΔTLDc) were synthesized by GeneScript, and inserted in expression plasmid pEGFP-N1 between Xho I and BamHI sites. The constructs pEGFP-N-hOXR1A and pEGFP-N-OXR1A ΔTLDc consist of exon 1-16 and 1-12, respectively. Similarly, the cDNA of OXR1A and OXR1A ΔTLDc were inserted into plasmid pET28b and fused with the Hisx6 Tag between the Nde I and BamHI sites to obtain pET28b-OXR1A and pET28b-OXR1A ΔTLDc plasmids. All the plasmids were verified by sequencing. The pEGFP-N-OXR1A and -OXR1A ΔTLDc plasmids were transfected into GH3 and U2OS cells by Lipofectamine 3000 Reagent (Thermo Fisher Scientific). The plasmids of pET28b-OXR1A and -OXR1A ΔTLDc were transformed into *E. coli* and further used for purification of recombinant hOXR1 proteins.

Mass spectrometry for identification of OXR1A interaction partners

The human plasmids pEGFP-N-OXR1A was transfected into the human cell line U2OS to establish cell lines stably expressing OXR1A-GFP proteins. Cells from T75 flasks were collected and proteins from cell extract were pulled down using a GFP-Trap M kit (Chromotek). The OXR1 binding proteins were identified and quantified by a MS instrument QExactive with Easy nanoLC (Thermo

Scientific). The proteins with average enrichment from triplicate samples larger than 5-fold as compared to control (only expression of GFP) are considered as OXR1 interaction partners. p value at < 0.01.

Targeted mass spectrometry

Sample preparation for targeted mass spectrometry: After above immunoprecipitation of OXR1 and its partners from U2OS extract, the GFP-Trap beads were washed and kept in 20 μL of 50 mM NH_4HCO_3 containing 2 mM DTT. Alkylation was performed by adding 1 μL of a 100 mM iodoacetamide to the beads followed by incubation for 40 min at room temperature in the dark. The reaction was quenched with 1 μL of 100 mM DTT for 20 min. 0.4 μg Trypsin (Thermo Scientific) was added to the samples following by overnight incubation at 37°C in a shaker. Subsequently, the elution containing the generated tryptic peptides were collected and 0.1% formic acid was added to a final volume of 40 μL. Finally, 12 μL of each sample were transferred to vials containing 10 fmol of the heavy standards pool and analyzed by targeted mass spectrometry.

Peptide standards for targeted mass spectrometry: Synthetic peptides containing heavy labeled Lysine (+8) or Arginine (+10) (PEPotec SRM Grade 2 Peptides, Thermo scientific) were used for method development and as internal standards for chromatographic quality control. The synthetic peptides used in this study were in Table S9.

Targeted MS: All parallel reaction monitoring (PRM)-based targeted mass spectrometry methods were designed, analyzed, and processed using Skyline software version 4.1.0.11714 (MacLean et al., 2010). *In silico* selection of proteotypic peptides was performed via Skyline using the *Homo sapiens* reference proteome available at https://www.uniprot.org:443/ to exclude non-unique peptides. Peptide standards were first analyzed on a Thermo Scientific Q Exactive HF mass spectrometer operating in PRM mode. This data was imported into skyline and used for the selection of the top ionizing peptides (2+ and 3+ charge states) and to build a scheduled method with retention time windows of 5 min. The method was then employed for detection and quantification of corresponding peptides in the samples. The information on retention time and fragmentation pattern of the heavy labeled peptide standards was used for peptide identification. The instrument parameters described below for sample analysis were adopted for establishment of the PRM method with standard peptides: Tryptic digests were analyzed on a Q Exactive HF mass spectrometer operating in PRM mode coupled to an EASY-nLC 1200 UHPLC system (Thermo Scientific). Peptides were injected onto an Acclaim PepMap C18 column (75 μm i.d. × 2 cm nanoviper, 3 μm particle size, 100 Å pore size) (Thermo Scientific) and further separated on an EASY Spray™ LC column (75 μm i.d. × 50 cm nanoviper, 2 μm particle size, 100 Å pore size) (Thermo Scientific) at 40°C. The following 120 min method was used at 300 nl/min flow rate: starting with 6% buffer B (80% Acetonitrile, 0.1% Formic acid) with an increase to 31% buffer B in 105 min, followed by an increase to 100% Buffer B over 6 min, where it was subsequently held for 9 min. Buffer A consisted of 0.1% Formic acid. The peptides eluting from the column were ionized by an Easy Spray™ Source (Thermo Scientific) and analyzed on positive-ion mode using electrospray voltage 1.75 kV and HCD fragmentation. Each MS/MS scan was acquired at a resolution of 60 000 FWHM, normalized collision energy (NCE) 28, automatic gain control (AGC) target value of 2×10^5, maximum injection time (mIT) of 110 ms and isolation window 1.4 m/z.

Protein Quantification: Heavy labeled peptides were spiked into the samples and used for chromatography quality control and peptide identification. However, due to the high concentration of internal standards in relation to endogenous peptides, quantification of endogenous peptides was not based on heavy/light ratios. Instead, quantification of peptides detected in the samples was achieved by summing the integrated peak areas of the most intense fragments. Peptide areas for multiple peptides of the same protein were summed to assign relative abundance to that protein. To evaluate the levels of each protein in distinct groups, values of relative abundance of each protein in samples belonging to the same group were averaged. Each group consists of 3 biological replicates. A minimum of 2 peptides per protein was used for quantification.

Immunofluorescent staining

The cells were fixed with 4% paraformaldehyde, permeabilized with 0.1% Triton X-100 in PBS. The cells were subsequently incubated in the presence of blocking buffer containing 5% goat serum, 5% bovine serum albumin and 0.1% Tween 20 in PBS for 30 min followed by incubation with primary antibodies diluted in PBS buffer containing 0.5% goat serum, 0.5% bovine serum albumin and 0.1% Tween 20 at 4°C overnight. After three washes in PBS containing 0.1% Tween 20, staining with secondary antibodies was performed for 60 min at room temperature in the dark. After three washes in PBS containing 0.1% Tween 20 (10 min each) and once in PBS, the slides were mounted with Duolink® *In Situ* Mounting Medium with DAPI (Cat. No. DUO82040, SIGMA). Microscopy was carried out using a Leica SP8 confocal microscope equipped with × 40 oil immersion lens. The antibodies used were anti-PRMT5 (anti-PRMT5, 1:200), anti-Growth hormone antibody (1:200-400), Anti-Rabbit IgG–Cy3 antibody produced in sheep (1:500), Donkey anti-Goat IgG (H+L) Cross-Adsorbed Secondary Antibody, Alexa Fluor 488 (1:500), Alexa Fluor® 488 Goat Anti-Rabbit IgG (1:500), Alexa Fluor® 594 Goat Anti-Mouse IgG (1:500).

Isotope C^{14} SAM based methylation assay

The assay was performed in a total reaction volume of 15 μL reaction including 1x PBS buffer, 5 μg Histone H3 from calf thymus (Sigma Aldrich, 11034758001), recombinant PRMT5/MEP50 complex (Active motif, Catalog No: 31356), 5 nmol [^{14}C] SAM (Adenosyl -L-Methionine, S-[methyl-14C]-, 10μCi (370kBq), Perkin Elmer). Added 1 μl purified OXR1A protein (concentration as indicated) or 1 μl BSA (concentration as indicated, dissolved in the same buffer as OXR1A) and incubated for 1 h at RT. Added 5 μl 4xNuPAGE

buffer to reaction mixtures, heated at 65°C 5 min, loaded on a 4%–15% SDS-PAGE, dried the gel on filter paper, exposed the gel on a low energy storage phosphor screen (GE) for 3 days at RT. Methylated histone H3 was detected by Typhoon imager (GE).

Antibody-based methylation assay

In vitro histone H3 mono- and di-methylation assay was also performed using recombinant human histone H3 (Recombinant Histone H3 (C110A), Catalog No: 31207, Active motif). Histone H3 (1.5 μg) was incubated with recombinant PRMT5/MEP50 complex (52.5ng), and either 1 μl purified OXR1A protein (concentration as indicated) or protein buffer (same as OXR1A dissolved in) in a 30 μl reaction mixture of PBS buffer containing 0.6 nmol SAM (S-adenosylmethionine, New England Biolabs) for 1 hour at RT. Added 10 μl 4xNu-PAGE buffer to reaction mixtures, heated at 65°C 5 min and loaded on a 4%–15% SDS-PAGE. The following steps were done according to western blot described above. The mono-methylation at Arg-2 of Histone H3 was detected by anti-Histone H3 (mono methyl R2) antibody (ab15584, abcam, 1:300), and symmetric dimethylation at Arg-2 (H3R2) was detected by anti- Histone H3R2 Symmetric Dimethyl Polyclonal Antibody (A-3705-100, Epigentek, 1:1000).

Methylation assays with H3 N-terminal tail (aa 1-21) peptides

In vitro methylation assays with 7.35 nM PRMT5/MEP50 complex (Active motif, Catalog No: 31356), 0.4 μM N-terminal H3 peptides (H3(1-21) WT, H3(1-21)_R8K/R17K or H3(1-21)_R2K/R8K/R17K),with and without OXR1A (29 nM) or truncated OXR1A (29 nM, OXR1A ΔTLDc) were carried out in 50 mM HEPES (pH 8.0), 10 mM NaCl, and 1 mM DTT containing [3H] SAM (25:1 molar ratio of SAM(B9003S, NEB) to [methyl-3H]-SAM (NET155001MC, PerkinElmer). Reactions were incubated for 1 h at 37°C, and then quenched with 0.5 μL of 100% (vol/vol) TFA. Each reaction was run in quadruplicate. Twenty-five microliters of each reaction were transferred to MilliporeSigma MultiScreenHTS 96-Well Filter Plates with Negatively Charged Membrane (10245703) and air-dried for 30 min. The papers were subsequently washed in 50 mM NaHCO3 at pH 9.0 for 45 min as previously described (Jain et al., 2017), and according to the manufacturing introduction. Radioactivity was counted using a 1450 MicroBeta Instrument (Wallac at Department of Immunology and Transfusion Medicine, Oslo University Hospital, Oslo, Norway), as previously described (Fauskanger et al., 2018).

Generation of rat OXR1 knockout cell line

The guiding RNA (gRNA) oligos were designed using CRISPR Design Tool (Hsu et al., 2013), gRNAs that target exon 3, 5 and 15, and with low off target predictions were selected. The oligos (aaacGGGTTCAACCCTTTGGGTGGc, aaacGGGTTCAACCCTTTGGGTGGc, caccgGTATATTCAATAGTTCCCTT, caccgGTATATTCAATAGTTCCCTT, aaacAAGGGAACTATTGAATATACc, caccgGACATGGATTCGTTAGCGTT, aaacAACGCTAACGAATCCATGTCc) were purchased from Sigma, and cloned into and plasmid pLentiCRISPER V2 according to protocol (Shalem et al., 2014). To make lentiviruses, 2 μg of pLentiCRISPER V2 was co-transfected with 3 μg of Trans-lentivirak packaging Mix (TLP4606, Thermo Scientific) into 2x10^6 HEK293T cells (Open Biosystem) seeded in 6 well trays, by using X-tremeGENE HP DNA Transfection Reagent (Roche). 24-72 hour after co-transfection, steril-filtered (40 μm) media from the HEK293T culture was transferred to 12 well trays containing 1x10^5 GH3 cells/well. Infected cells were selected by using 2 μg/ml Puromycine (Invitrogen) in F12K media supplemented with 20% FCS (Sigma) and 2 mM L-Glutamine (Sigma). After 7 −10 days of selection, cells were sub-cloned and screened by western blot using anti OXR1 antibody (OXR1 Ab1, N106.1).

Mouse GH ELISA assay

Circulating levels of GH were assayed by ELISA. We fasted 6-month-old WT and *Oxr1A* $^{-/-}$ mice, eight mice in each group, for 4 hours from 7 am. We collected blood samples at −30 and 5, 30, and 240 min from Lateral saphenous vein with Microvette® tubes (Microvette® CB 300 μl, K2 EDTA, violet US code, Sarstedt), 50 μl each time, and monitored glucose level before and after fasting. The blood samples were centrifuged at 12,000 rpm for 5 min at 4°C, and the plasma samples were collected and stored at −80°C. The plasma GH concentration was measured using commercially available ELISA kit (EZRMGH-45K, Millipore Co) according to the manufacturer's instructions. Absorbance for GH was measured and analyzed using a standard curve. We analyzed the individual provocative growth hormone response by calculation the ratio of peak and basal level of GH concentrations.

Chromatin immunoprecipitation (CHIP)

For CHIP experiments, the cells were harvested by trypsin digestion and crosslinked using formaldehyde (1% final, Sigma) in normal culture medium for 10 min at room temperature. The cells were washed twice with cold PBS. The cells were lysed and chromatin was prepared using a Chromatin extraction kit (abcam, Ab117152). The chromatin was sheared to an average size at 250-300 bp using a Bioruptor Pico (Diagenode) in a 0.65 mL tube for 10 cycles (each cycle was 30 s on and 30 s off). IP was performed using a CHIP kit Magnetic-One-Step (abcam, ab156907). Briefly, a total of 3-6 μg chromatins were mixed with 1 μg antibody or IgG in CHIP buffer (total 100 μL per reaction). The mixture was incubated on a rolling shaker for 120 min at 4°C. The reaction was washed 4 times with washing buffer, once by DNA release buffer, and eluted by adding 39 μL DNA release buffer and 1 μL proteinase K. The cross-links were reversed by incubating the elution sample at 65°C 15 min and then 95°C 10 min in a thermal cycler. The input was prepared by adding 90 μl DNA release buffer in 10 μL chromatin sample following reversal of crosslinks as above.

Histological staining in liver tissues

Liver tissue isolated from WT and *Oxr1A*$^{-/-}$ mice was fixed in 4% formalin and embedded in paraffin for histological analysis. Liver Sections (4 μm) were deparaffinized and stained with hematoxylin (Vector Laboratories Inc.) and eosin (Histolab). Images were captured by use of a Nikon DS Fi1 camera and a Nikon Eclipse E400 microscope.

Hepatic triglyceride (TG) and cholesterol (CHOL) measurements

Liver lipid extraction was performed and cholesterol and TG levels were quantified by use of enzymatic colorimetric kits (Wako Chemical GmbH, Neuss, Germany) according manufacturers protocol.

Activities of murine liver enzymes involved in FA metabolism

The liver enzyme activity was measured by carnitine palmitoyl transferase assay for CPT-1,2, by spectrophotometric assay for FAO (fatty acyl-CoA oxidase) (Øie et al., 2013).

Oral Glucose Tolerance Test and Blood glucose measurement

Oral glucose tolerance test was performed on both WT and *Oxr1A*$^{-/-}$ mice. Mice were fasted for 4 hours; fasted glucose values were determined and subsequently were given an oral dose of glucose (2 mg/kg of body weight). Blood glucose values were measured 20, 40, 60, 90 and 120 min after glucose ingestion. Glucose concentrations were measured in venous blood with a glucometer (Accu-Chek Aviva, Roche, Basel, Switzerland).

QUANTIFICATION AND STATISTICAL ANALYSIS

Each assay consists of at least three independent experiments with technical triplicates except those described specifically. The results are presented as average values with SD unless otherwise stated. Statistical analysis was performed by calculating p values using Student's t test with two tailed distribution between groups assuming equal variances. A confidence level of 95% (*$p < 0.05$; **$p < 0.01$) was considered statistically significant.

DATA AND CODE AVAILABILITY

ACCESSION NUMBERS: mouse liver raw RNA-seq data were deposited to Gene Expression Omnibus database (GEO: GSE97024).